

Electronic supplementary information

meso-Ethynyl-extended push-pull type porphyrins for near-infrared organic photodetectors

Sam Gielen, Virginia Cuesta Gómez, Sonny Brebels, Tyler James Quill, Jochen Vanderspikken, Laurence Lutsen, Pilar de la Cruz, Koen Vandewal, Fernando Langa, Wouter Maes

Table of contents

<u>Section 1</u> : Synthesis and characterization (strategy 1)	S2
1.1. Materials and methods	S2
1.2. Synthesis and characterization of the precursors and <i>meso</i> -ethynyl-extended porphyrin chromophores for strategy 1	S3
1.3. ¹ H-NMR, ¹³ C-NMR, and MALDI-ToF mass spectra	S9
1.4. UV-VIS-NIR absorption spectra	S19
1.5. Cyclic voltammetry	S19
<u>Section 2</u> : Device characterization and optimization	S20
2.1. Organic photodetector fabrication and characterization	S20
2.2. Device optimization and characterization	S21
<u>Section 3</u> : Synthesis and characterization of the precursors for strategy 2 and TII-Por-TII	S28
3.1. Materials and methods	S28
3.2. Synthesis and characterization of the precursors, the ethynyl-extended acceptor chromophores, and TII-Por-TII	S28
3.3. ¹ H-NMR, ¹³ C-NMR, and MALDI-ToF mass spectra	S33
References	S37

Section 1: Synthesis and characterization (strategy 1)

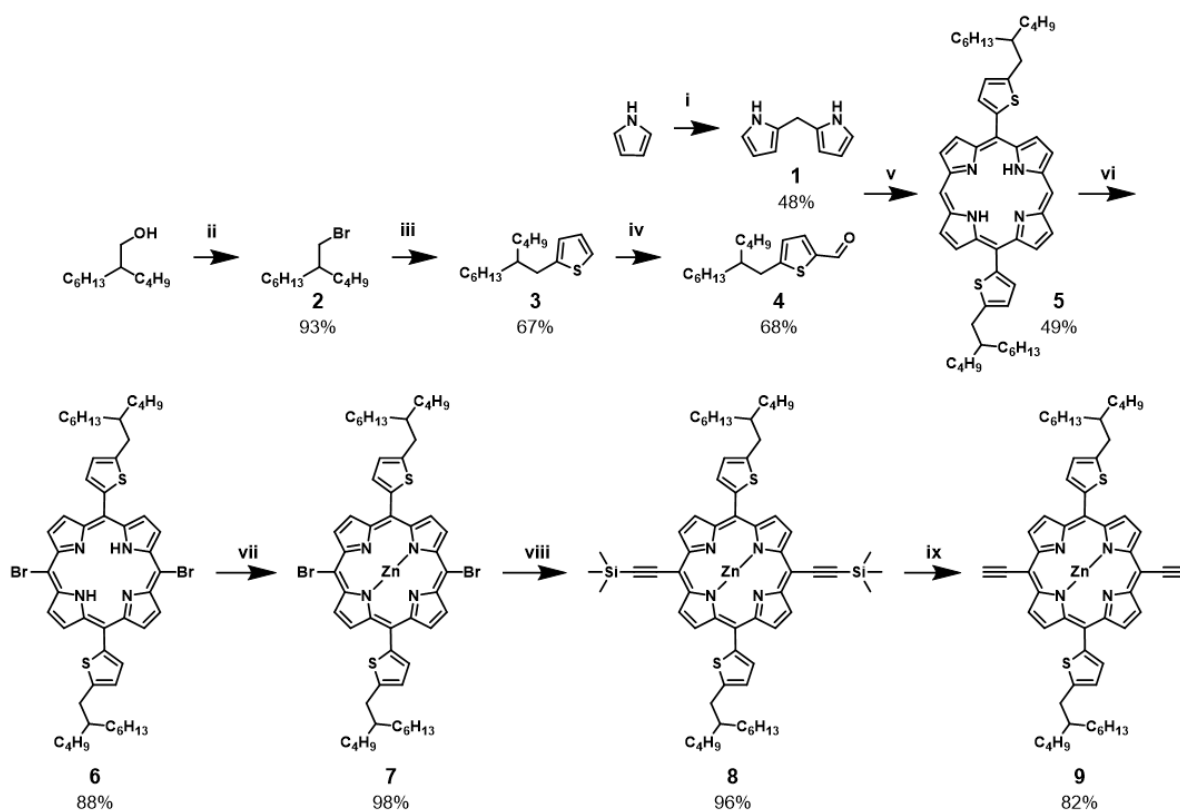
1.1. Materials and methods

Preparative (recycling) size exclusion chromatography (prep-SEC) was performed on a JAI LC-9110 NEXT system equipped with JAIGEL 1H and 2H columns (eluent CHCl_3 , flow rate 3.5 mL min^{-1}). NMR chemical shifts (δ , in ppm) were determined relative to the residual CHCl_3 (7.26 ppm) or THF (1.73 and 3.58 ppm) signals or the ^{13}C resonance shift of CDCl_3 (77.16 ppm). Matrix-assisted laser desorption/ionization - time-of-flight (MALDI-ToF) mass spectra were recorded on a Bruker UltrafleXtreme™ MALDI-TOF/TOF system. Approximately $1 \mu\text{L}$ of the matrix solution (25 mg mL^{-1} *trans*-2-[3-(4-*tert*-butylphenyl)-2-methyl-2-propenylidene]malononitrile (DTCB) in chloroform) was spotted onto an MTP Anchorchip 600/384 MALDI plate. The spot was allowed to dry and $1 \mu\text{L}$ of the analyte solution (10 mg mL^{-1} in chloroform) was spotted on top of the matrix. High resolution electrospray ionization mass spectrometry (ESI-MS) was performed using an LTQ Orbitrap Velos Pro mass spectrometer equipped with an atmospheric pressure ionization source operating in the nebulizer assisted electrospray mode. The instrument was calibrated in the m/z range 220–2000 using a standard solution containing caffeine, MRFA, and Ultramark 1621. UV-VIS-NIR absorption spectroscopy measurements were performed on a VARIAN Cary 5000 UV-VIS-NIR spectrophotometer at a scan rate of 600 nm min^{-1} . The films for the UV-VIS-NIR absorption measurements were prepared by spin-coating a solution of the respective porphyrin molecule in chloroform on a glass substrate. The solid-state UV-VIS-NIR absorption spectra were used to estimate the optical gaps (from the wavelength at the intersection of the tangent line drawn at the low energy side of the absorption spectrum with the baseline: $E_g \text{ (eV)} = 1240/(\text{wavelength in nm})$). Electrochemical measurements (cyclic voltammetry, CV) were performed with an Eco Chemie Autolab PGSTAT 30 potentiostat/galvanostat using a three-electrode microcell with a platinum working electrode, a platinum counter electrode, and an Ag/AgNO₃ reference electrode (silver wire dipped in a solution of 0.01 M AgNO₃ and 0.1 M NBu₄PF₆ in anhydrous acetonitrile). The reference electrode was calibrated against ferrocene/ferrocenium as an external standard. Sample preparation was done by dip-coating the platinum working electrode in the respective polymer solutions. The CV measurements were done on the resulting films with 0.1 M NBu₄PF₆ in anhydrous acetonitrile as electrolyte solution. The experiments were carried out under a curtain of argon to prevent air from entering the system. Cyclic voltammograms were recorded at a scan rate of 100 mV s^{-1} . For the conversion of V to eV, the onset potentials of the first oxidation/reduction peaks were used and referenced to ferrocene/ferrocenium, which has an ionization potential of -4.98 eV vs. vacuum. This correction factor is based on a value of 0.31 eV for Fc/Fc⁺ vs. SCE and a value of 4.68 eV for SCE vs. vacuum: $E_{\text{HOMO/LUMO}} \text{ (eV)} = -4.98 - E_{\text{onset ox/red}}^{\text{Ag/AgNO}_3} \text{ (V)} + E_{\text{onset Fc/Fc}^+}^{\text{Ag/AgNO}_3} \text{ (V)}$.^{1, 2} The accuracy of measuring redox potentials by CV is about 0.01–0.02 V.

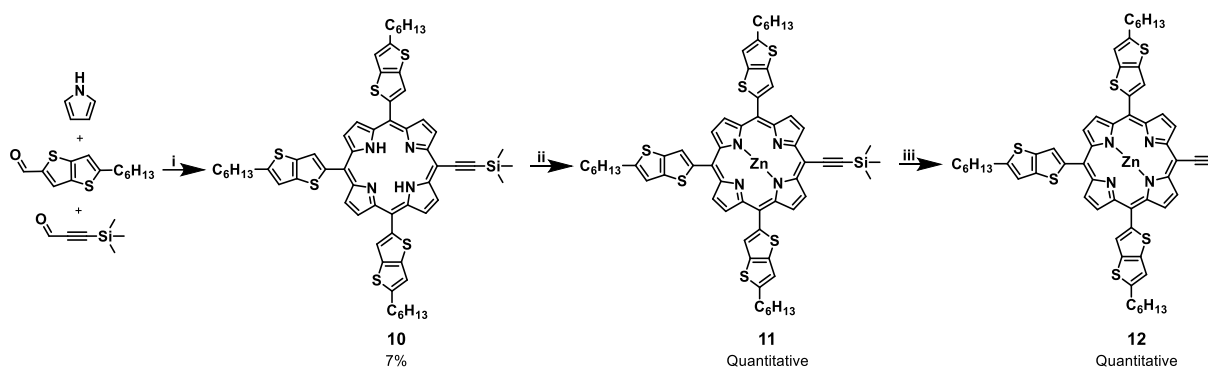
Reproducibility issues can occur due to the dependence of the potentials on concentration and temperature.

1.2. Synthesis and characterization of the precursors and *meso*-ethynyl-extended porphyrin chromophores for strategy 1

All reagents and chemicals were obtained from commercial sources and used without further purification, except for pyrrole which was freshly distilled before use. Solvents were dried on a solvent purification system (MBraun, MB-SPS-800) equipped with alumina columns. The 5,15-dialkynated porphyrin **9** (Scheme S1)³, A₃B-porphyrin **12** (Scheme S2)⁴, and the acceptor molecules⁵⁻⁷ were prepared according to literature procedures.

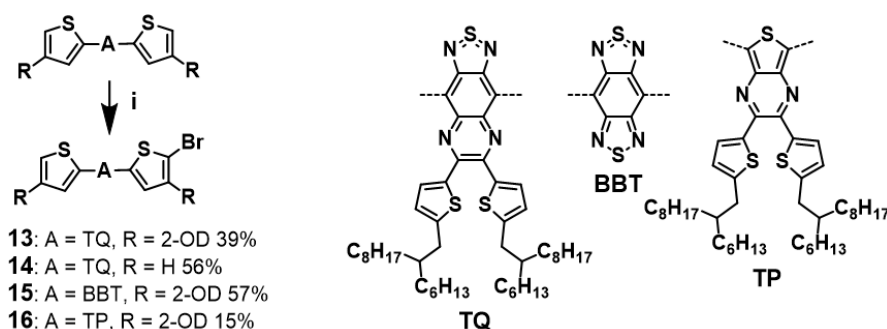


Scheme S1: Synthetic pathway toward 5,15-meso-ethynylporphyrin **9**: i) paraformaldehyde, TFA, RT; ii) NBS, PPh₃, CH₂Cl₂, RT; iii) thiophene, *n*-BuLi, THF, -78 °C to RT; iv) POCl₃, DMF, reflux; v) (1) BF₃·Et₂O, CHCl₃, RT; (2) DDQ; vi) NBS, pyridine, CHCl₃, RT; vii) Zn(OAc)₂, CHCl₃/MeOH, 70 °C; viii) TMS-acetylene, PdCl₂(PPh₃)₂, CuI, Et₃N, THF, 50 °C; ix) TBAF, THF, RT.



Scheme S2: Synthetic pathway toward mono-alkynated A_3B -porphyrin **12**: i) (1) $\text{BF}_3 \cdot \text{EtO}_2$, CHCl_3 , RT; (2) DDQ ; ii) $\text{Zn}(\text{OAc})_2$, $\text{CHCl}_3/\text{MeOH}$, RT; iii) TBAF , THF , RT.

General monobromination procedure: The acceptor material was dissolved in CHCl_3 and the solution was cooled down to 0°C while stirring. Then, NBS (1 equiv.) was added portionwise and the mixture was stirred overnight, slowly heating up to room temperature. The solvents were removed and column chromatography (silica, CHCl_3 :petroleum ether mixture) was performed to yield the pure product.



Scheme S3: Monobromination of the acceptor molecules: i) NBS (1 equiv), CHCl_3 , RT.

4-(5-bromo-4-(2-octyldodecyl)thiophen-2-yl)-6,7-bis(5-(2-hexyldecyl)thiophen-2-yl)-9-(4-(2-octyldodecyl)thiophen-2-yl)[1,2,5]thiadiazolo[3,4-g]quinoxaline (13). Column chromatography (CHCl_3 :petroleum ether, 1:4) was performed to yield the pure product as a purple oil. Yield = 39% (135 mg). $^1\text{H-NMR}$ (400 MHz, CDCl_3), δ (ppm): 8.74 (s, 2H), 7.48 (d, $J = 3.6$ Hz, 1H), 7.46 (d, $J = 3.6$ Hz, 1H), 7.26 (s, 1H), 6.73 (d, $J = 3.6$ Hz, 1H), 6.71 (d, $J = 3.6$ Hz, 1H), 2.86 (d, $J = 6.8$ Hz, 2H), 2.84 (d, $J = 6.8$ Hz, 2H), 2.71 (d, $J = 6.8$ Hz, 2H), 2.65 (d, $J = 6.8$ Hz, 2H), 1.88–1.70 (m, 4H), 1.40–1.15 (m, 112H), 0.90–0.80 (m, 24H). $^{13}\text{C-NMR}$ (100 MHz, CDCl_3): δ (ppm) = 152.6, 152.3, 152.0, 152.0, 146.7, 146.5, 142.3, 141.3, 139.9, 139.6, 136.0, 135.9, 135.9, 135.0, 134.8, 134.7, 132.5, 132.4, 128.0, 126.5, 126.4, 121.0, 119.6, 118.3, 40.6, 39.6, 39.2, 35.6, 34.7, 33.9, 32.5, 30.6, 30.2, 29.9, 27.2, 23.2, 14.7. MALDI-ToF MS (m/z): calculated for $\text{C}_{96}\text{H}_{155}\text{BrN}_4\text{S}_5$: 1603.00 [M] $^+$; found 1603.01.

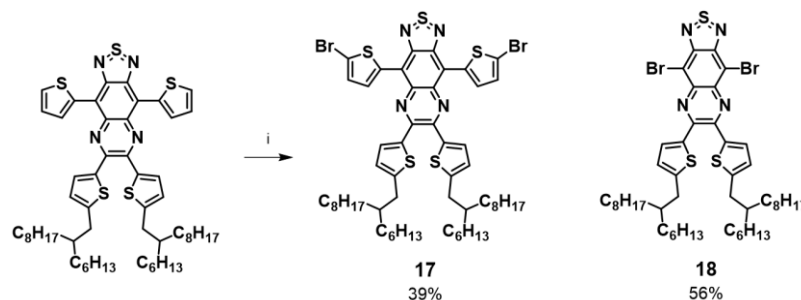
4-(5-bromothiophen-2-yl)-6,7-bis(5-(2-hexyldecyl)thiophen-2-yl)-9-(thiophen-2-yl)[1,2,5]thiadiazolo[3,4-g]quinoxaline (14). Column chromatography (CHCl_3 :petroleum ether, 1:4) was performed to yield the pure product as a purple oil. Yield = 56% (374 mg). $^1\text{H-NMR}$ (400 MHz, CDCl_3): δ (ppm) = 8.89

(dd, $J = 3.9, 1.2$ Hz, 1H), 8.80 (d, $J = 4.2$ Hz, 1H), 7.70 (dd, $J = 5.2, 1.2$ Hz, 1H), 7.49–7.46 (m, 2H), 7.31 (dd, $J = 5.2, 3.9$ Hz, 2H), 7.25 (1H), 6.74 (d, $J = 3.8$ Hz, 1H), 6.71 (d, $J = 3.8$ Hz, 1H), 2.87 (d, $J = 6.7$ Hz, 2H), 2.84 (d, $J = 6.7$ Hz, 2H), 1.80–1.70 (m, 2H), 1.40–1.20 (m, 48H), 0.91–0.81 (m, 12H). $^{13}\text{C-NMR}$ (100 MHz, CDCl_3): δ (ppm) = 151.9, 151.6, 151.2, 146.3, 146.1, 139.4, 139.1, 137.5, 135.8, 135.9, 134.1, 133.9, 133.2, 133.0, 132.2, 132.1, 131.2, 129.5, 126.8, 126.0, 120.5, 119.7, 119.1, 40.2, 40.1, 35.1, 35.0, 33.5, 32.1, 30.2, 30.1, 29.8, 29.5, 26.8, 22.8, 14.3. ESI-MS (m/z): calculated for $\text{C}_{56}\text{H}_{75}\text{BrN}_4\text{S}_5$: 1042.3779 $[\text{M}]^+$; found 1042.3776.

4-(5-bromo-4-(2-octyldodecyl)thiophen-2-yl)-8-(4-(2-octyldodecyl)thiophen-2-yl)-1H,5H-benzo[1,2-*c*:4,5-*c'*]bis([1,2,5]thiadiazole) (15). Column chromatography (CHCl_3 :petroleum ether, 15:85) was performed to yield the pure product as a blue solid. Yield = 57% (82 mg). $^1\text{H-NMR}$ (400 MHz, CDCl_3): δ (ppm) = 8.72 (d, $J = 1.1$ Hz, 1H), 8.55 (s, 1H), 7.24 (1H), 2.69 (d, $J = 6.7$ Hz, 2H), 2.61 (d, $J = 6.7$ Hz, 2H), 1.85–1.78 (br, 1H), 1.77–1.71 (br, 1H), 1.40–1.15 (m, 64H), 0.90–0.80 (m, 12H). $^{13}\text{C-NMR}$ (100 MHz, CDCl_3): δ (ppm) = 150.8, 150.5, 143.0, 142.1, 137.1, 137.0, 134.9, 133.8, 127.6, 117.6, 113.7, 111.9, 39.1, 38.7, 35.1, 34.2, 33.5, 32.0, 30.2, 29.9, 29.8, 29.8, 29.5, 29.5, 26.8, 26.7, 22.8, 14.2. ESI-MS (m/z): calculated for $\text{C}_{54}\text{H}_{85}\text{BrN}_4\text{S}_4$: 996.4840 $[\text{M}]^+$; found 996.4837.

5-(5-bromo-4-(2-octyldodecyl)thiophen-2-yl)-2,3-bis(5-(2-hexyldecyl)thiophen-2-yl)-7-(4-(2-octyldodecyl)thiophen-2-yl)thieno[3,4-*b*]pyrazine (16). Column chromatography (CHCl_3 :petroleum ether, 5:95) was performed to yield the pure product as a green solid. Yield = 15% (41 mg). $^1\text{H-NMR}$ (400 MHz, CDCl_3), δ (ppm): 7.42 (d, $J = 1.1$ Hz, 1H), 7.26 (d, $J = 3.6$ Hz, 1H), 7.23 (d, $J = 3.8$ Hz, 1H), 7.18 (s, 1H), 6.94 (d, $J = 1.1$ Hz, 1H), 6.66 (d, $J = 3.8$ Hz, 1H), 6.64 (d, $J = 3.8$ Hz, 1H), 2.81–2.79 (m, 4H), 2.55 (d, $J = 6.8$ Hz, 2H), 2.50 (d, $J = 6.8$ Hz, 2H), 1.75–1.60 (m, 4H), 1.40–1.16 (m, 112H), 0.92–0.80 (m, 24H). $^{13}\text{C-NMR}$ (100 MHz, CDCl_3): δ (ppm) = 149.9, 149.7, 146.3, 142.1, 142.4, 141.3, 140.1, 140.0, 136.7, 136.3, 134.2, 134.2, 130.5, 130.4, 126.6, 125.8, 125.0, 124.6, 122.9, 122.8, 112.0, 40.1, 40.0, 39.0, 38.7, 35.0, 35.0, 34.3, 33.4, 32.0, 30.2, 29.8, 29.5, 26.8, 26.7, 22.8, 14.2. ESI-MS (m/z): calculated for $\text{C}_{94}\text{H}_{155}\text{BrN}_2\text{S}_5$: 1550.00 $[\text{M}]^+$; found 1550.01.

Dibromination procedure: The dibrominated acceptor molecules (Scheme S4) were prepared according to literature procedures.^{7,8}

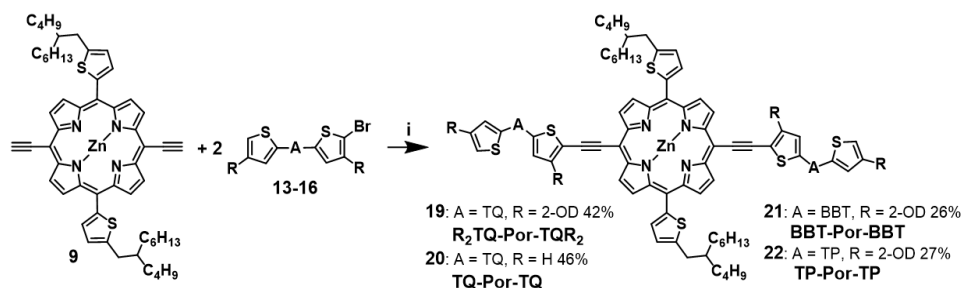


Scheme S4: Dibrominated acceptor molecules for the preparation of the D-A-D chromophores: i) NBS (2 equiv), CHCl_3 , RT.

4,9-bis(5-bromothiophen-2-yl)-6,7-bis(5-(2-hexyldecyl)thiophen-2-yl)-[1,2,5]thiadiazolo[3,4-g]quinoxaline (17).⁷ Quantitative yield (6.65 g). $^1\text{H-NMR}$ (400 MHz, CDCl_3): δ (ppm) = 8.79 (d, J = 4.2 Hz, 2H), 7.47 (d, J = 3.8 Hz, 2H), 7.24 (d, J = 4.2 Hz, 2H), 6.74 (d, J = 3.8 Hz, 2H), 2.87 (d, J = 6.6 Hz, 4H), 1.81–1.73 (m, 2H), 1.41–1.20 (m, 48H), 0.89–0.81 (m, 12H). $^{13}\text{C-NMR}$ (100 MHz, CDCl_3): δ (ppm) = 151.9, 151.1, 146.2, 139.0, 137.4, 133.5, 133.2, 132.3, 129.5, 126.0, 120.0, 119.0, 40.2, 35.1, 33.5, 32.1, 30.1, 29.8, 29.5, 26.9, 26.8, 22.84, 22.82, 14.27, 14.25.

4,9-dibromo-6,7-bis(5-(2-hexyldecyl)thiophen-2-yl)-[1,2,5]thiadiazolo[3,4-g]quinoxaline (18).⁸ Yield = 28% (0.50 g). $^1\text{H-NMR}$ (400 MHz, CDCl_3): δ (ppm) = 7.51 (d, J = 3.8 Hz, 2H), 6.72 (d, J = 3.8 Hz, 2H), 2.82 (d, J = 6.7 Hz, 4H), 1.78–1.70 (m, 2H), 1.37–1.23 (m, 48H), 0.90–0.83 (m, 12H). $^{13}\text{C-NMR}$ (100 MHz, CDCl_3): δ (ppm) = 153.3, 152.3, 148.9, 139.2, 139.8, 132.4, 126.4, 112.5, 40.2, 35.2, 33.4, 32.01, 31.98, 30.1, 29.7, 29.5, 26.69, 26.66, 22.8, 14.2.

General Sonogashira cross-coupling procedure for the A-D-A type porphyrins: Porphyrin precursor **9** (1 equiv.) and the respective monobrominated acceptor molecule **13–16** (2.2 equiv.) were placed in a Schlenk flask and the flask was flushed three times with N_2 , after which dry toluene (7.3 mM) and dry Et_3N (3.7 mM) were added. Then, the mixture was purged with N_2 for 30 min. Afterwards, $\text{Pd}(\text{PPh}_3)_2\text{Cl}_2$ (0.05 equiv.) and CuI (0.05 equiv.) were added and the reaction was stirred overnight at 85 °C. Next morning, the reaction mixture was cooled down, water was added and extraction was done with CHCl_3 . The organic solution was dried over MgSO_4 , filtered and evaporated to dryness. Flash column chromatography (silica) was performed with CHCl_3 :petroleum ether (3:1), followed by preparative (recycling) SEC to yield the product as a dark brown solid.



Scheme S5: Sonogashira cross-coupling reaction of alkyne **9** and monobrominated acceptor molecules **13–16**: i) $\text{PdCl}_2(\text{PPh}_3)_2$, CuI , Et_3N , toluene, 85°C .

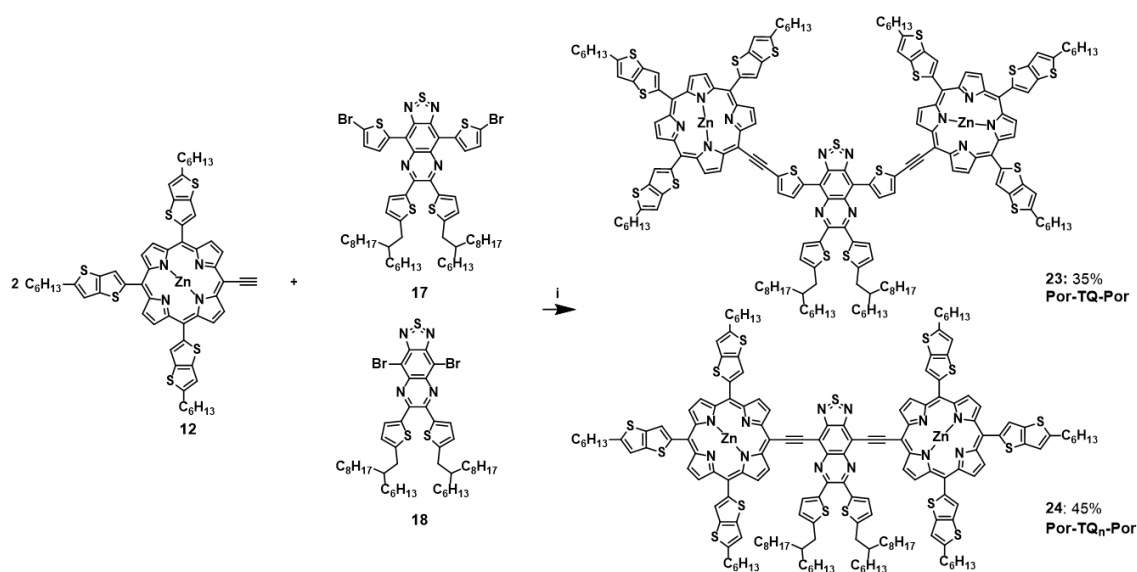
R₂TQ-Por-TQR₂ (19). Yield = 42% (49 mg). $^1\text{H-NMR}$ (400 MHz, $\text{CDCl}_3/\text{CS}_2$), δ (ppm): 9.70 (s, 4H), 9.15 (d, $J = 4.6$ Hz, 4H), 9.06 (s, 2H), 8.78 (s, 2H), 7.71 (d, $J = 3.2$ Hz, 2H), 7.61 (d, $J = 3.7$ Hz, 2H), 7.56 (d, $J = 3.7$ Hz, 2H), 7.23 (s, 2H), 7.17 (d, $J = 3.2$ Hz, 2H), 6.78 (d, $J = 3.6$ Hz, 2H), 6.75 (d, $J = 3.6$ Hz, 2H), 3.27 (d, $J = 6.4$ Hz, 4H), 3.10 (d, $J = 6.4$ Hz, 4H), 2.88 (d, $J = 6.4$ Hz, 4H), 2.87 (d, $J = 6.4$ Hz, 4H), 2.69 (d, $J = 6.4$ Hz, 4H), 2.27–2.16 (m, 2H), 2.00–1.90 (m, 2H), 1.82–1.74 (br, 4H), 1.70–1.15 (br, 256H), 1.00–0.50 (br, 60H). MALDI-ToF MS (m/z): calculated for $\text{C}_{248}\text{H}_{376}\text{N}_{12}\text{S}_{12}\text{Zn}$: 3966.54 [M]⁺; found 3966.55.

TQ-Por-TQ (20). Yield = 46% (213 mg). $^1\text{H-NMR}$ (400 MHz, $\text{CDCl}_3/\text{CS}_2$), δ (ppm): 9.30 (d, $J = 4.4$ Hz, 4H), 9.03 (d, $J = 4.4$ Hz, 4H), 8.90 (d, $J = 3.9$ Hz, 2H), 8.64 (d, $J = 3.0$ Hz, 2H), 7.75 (d, $J = 3.2$ Hz, 2H), 7.63 (d, $J = 3.6$ Hz, 2H), 7.60 (d, $J = 3.6$ Hz, 2H), 7.49–7.43 (m, 4H), 7.22 (d, $J = 3.3$ Hz, 2H), 7.07–7.02 (m, 2H), 6.84 (d, $J = 3.6$ Hz, 2H), 6.79 (d, $J = 3.6$ Hz, 2H), 3.16 (d, $J = 6.8$ Hz, 4H), 2.96 (d, $J = 6.8$ Hz, 4H), 2.91 (d, $J = 6.8$ Hz, 4H), 2.05–1.95 (m, 2H), 1.85–1.75 (m, 2H), 1.70–1.15 (br, 128H), 1.15–0.80 (br, 24H). 0.60 (t, $J = 7.1$ Hz, 6H), 0.55 (t, $J = 7.1$ Hz, 6H). MALDI-ToF MS (m/z): calculated for $\text{C}_{168}\text{H}_{212}\text{N}_{12}\text{S}_{12}\text{Zn}$: 2845.29 [M]⁺; found 2845.27.

BBT-Por-BBT (21). Yield = 26% (27 mg). $^1\text{H-NMR}$ (400 MHz, $\text{THF-}d_8$), δ (ppm): 10.81 (s, 2H), 9.05 (d, $J = 4.3$ Hz, 4H), 8.92 (d, $J = 4.3$ Hz, 4H), 8.73 (s, 2H), 8.54 (s, 2H), 7.38 (d, $J = 3.2$ Hz, 2H), 7.21 (s, 2H), 3.27 (d, $J = 6.2$ Hz, 8H), 2.67 (d, $J = 6.1$ Hz, 4H), 2.24–2.16 (m, 2H), 2.15–2.04 (m, 4H), 1.88–1.70 (m, 8H), 1.40–1.10 (br, 160H), 1.05–1.00 (t, $J = 7.2$ Hz, 12H), 0.88–0.82 (t, $J = 7.2$ Hz, 12H), 0.80–0.74 (m, 12H). MALDI-ToF MS (m/z): calculated for $\text{C}_{164}\text{H}_{232}\text{N}_{12}\text{S}_{10}\text{Zn}$: 2753.50 [M]⁺; found 2753.46.

TP-Por-TP (22). Yield = 27% (13 mg). $^1\text{H-NMR}$ (400 MHz, $\text{CDCl}_3/\text{CS}_2$), δ (ppm): 9.68 (d, $J = 4.6$ Hz, 4H), 9.14 (d, $J = 4.6$ Hz, 4H), 7.68 (d, $J = 3.2$ Hz, 2H), 7.64 (s, 2H), 7.46 (s, 2H), 7.33 (d, $J = 3.7$ Hz, 2H), 7.29 (d, $J = 3.7$ Hz, 2H), 7.15 (d, $J = 3.4$ Hz, 2H), 6.95 (s, 2H), 6.70 (d, $J = 3.6$ Hz, 2H), 6.67 (d, $J = 3.6$ Hz, 2H), 3.12 (d, $J = 6.8$ Hz, 4H), 3.07 (d, $J = 6.8$ Hz, 4H), 2.83 (d, $J = 6.8$ Hz, 4H), 2.81 (d, $J = 6.8$ Hz, 4H), 2.58 (d, $J = 6.8$ Hz, 4H), 2.13–2.02 (m, 2H), 1.97–1.85 (m, 2H), 1.78–1.66 (m, 6H), 1.40–0.95 (br, 256H), 0.91–0.85 (m, 30H), 0.75–0.62 (m, 30H). MALDI-ToF MS (m/z): calculated for $\text{C}_{244}\text{H}_{372}\text{N}_8\text{S}_{12}\text{Zn}$: 3862.53 [M]⁺; found 3862.52.

General Sonogashira cross-coupling procedure for the D-A-D type porphyrins: A₃B-porphyrin **12** (2.2 equiv.) and the respective dibrominated acceptor molecule **17** or **18** (1 equiv.) were placed in a Schlenk flask and the flask was flushed three times with N₂, after which dry toluene (7.3 mM) and dry Et₃N (3.7 mM) were added. Then, the mixture was purged with N₂ for 30 min. Afterwards, Pd(PPh₃)₂Cl₂ (0.05 equiv.) and CuI (0.05 equiv.) were added and the reaction was stirred overnight at 85 °C. Next morning, the reaction mixture was cooled down, water was added and extraction was done with CHCl₃. The organic solution was dried over MgSO₄, filtered and evaporated to dryness. Flash column chromatography (silica) was performed with CHCl₃:petroleum ether (3:1), followed by prep-SEC to yield the product as a dark brown solid.



Scheme S6: Final Sonogashira cross-coupling reaction of mono-alkynated A₃B-porphyrin **12** and dibrominated acceptor molecules **17-18**: i) PdCl₂(PPh₃)₂, CuI, Et₃N, toluene, 85 °C.

Por-TQ-Por (23). Yield = 35% (88 mg). ¹H-NMR (400 MHz, THF-*d*₈) δ(ppm): 9.53 (d, *J* = 4.4 Hz, 4H), 9.16 (d, *J* = 4.4 Hz, 4H), 9.10 (d, *J* = 4.5 Hz, 4H), 9.03 (d, *J* = 4.5 Hz, 4H), 8.14 (s, 4H), 8.11 (s, 2H), 7.81 (d, *J* = 3.6 Hz, 2H), 7.75–7.60 (br, 2H), 7.24 (s, 4H), 7.20 (s, 2H), 7.08 (d, *J* = 3.6 Hz, 2H), 6.75–6.60 (br, 2H), 3.19 (d, *J* = 6.5 Hz, 4H), 3.08 (t, *J* = 7.6 Hz, 8H), 2.98 (t, *J* = 7.4 Hz, 4H), 1.99–1.80 (m, 18H), 1.62–1.33 (m, 48H), 1.33–1.07 (m, 32H), 1.07–0.89 (m, 18H), 0.78–0.72 (m, 12H). MALDI-ToF MS (*m/z*): calculated for C₁₇₂H₁₈₀N₁₂S₁₇Zn₂: 3085 [M⁺]; found 3086.

Por-TQ_n-Por (24). Yield = 45% (55 mg). ¹H-NMR (400 MHz, THF-*d*₈) δ(ppm): 10.31 (s, 4H), 9.25 (d, *J* = 4.6 Hz, 4H), 9.05 (d, *J* = 4.6 Hz, 4H), 8.88 (d, *J* = 4.5 Hz, 4H), 8.13 (s, 4H), 7.67 (s, 2H), 7.54 (s, 2H), 7.32 (s, 4H), 7.15 (s, 2H), 6.80 (d, *J* = 3.5 Hz, 2H), 3.18 (t, *J* = 7.7 Hz, 8H), 3.05 (t, *J* = 7.7 Hz, 4H), 2.88 (d, *J* = 6.5 Hz, 4H), 2.00–1.94 (m, 8H), 1.92–1.85 (m, 8H), 1.66–1.64 (m, 2H), 1.48–1.42 (m, 32H), 1.35–1.33 (m, 48H), 1.03–0.98 (m, 18H), 0.78–0.70 (m, 12H). MALDI-ToF MS (*m/z*): calculated for C₁₆₄H₁₇₆N₁₂S₁₅Zn₂: 2920.85 [M⁺]; found 2920.89.

1.3. $^1\text{H-NMR}$, $^{13}\text{C-NMR}$, and MALDI-ToF mass spectra

4-(5-bromo-4-(2-octyldodecyl)thiophen-2-yl)-6,7-bis(5-(2-hexyldecyl)thiophen-2-yl)-9-(4-(2-octyldodecyl)thiophen-2-yl)[1,2,5]thiadiazolo[3,4-g]quinoxaline (**13**)

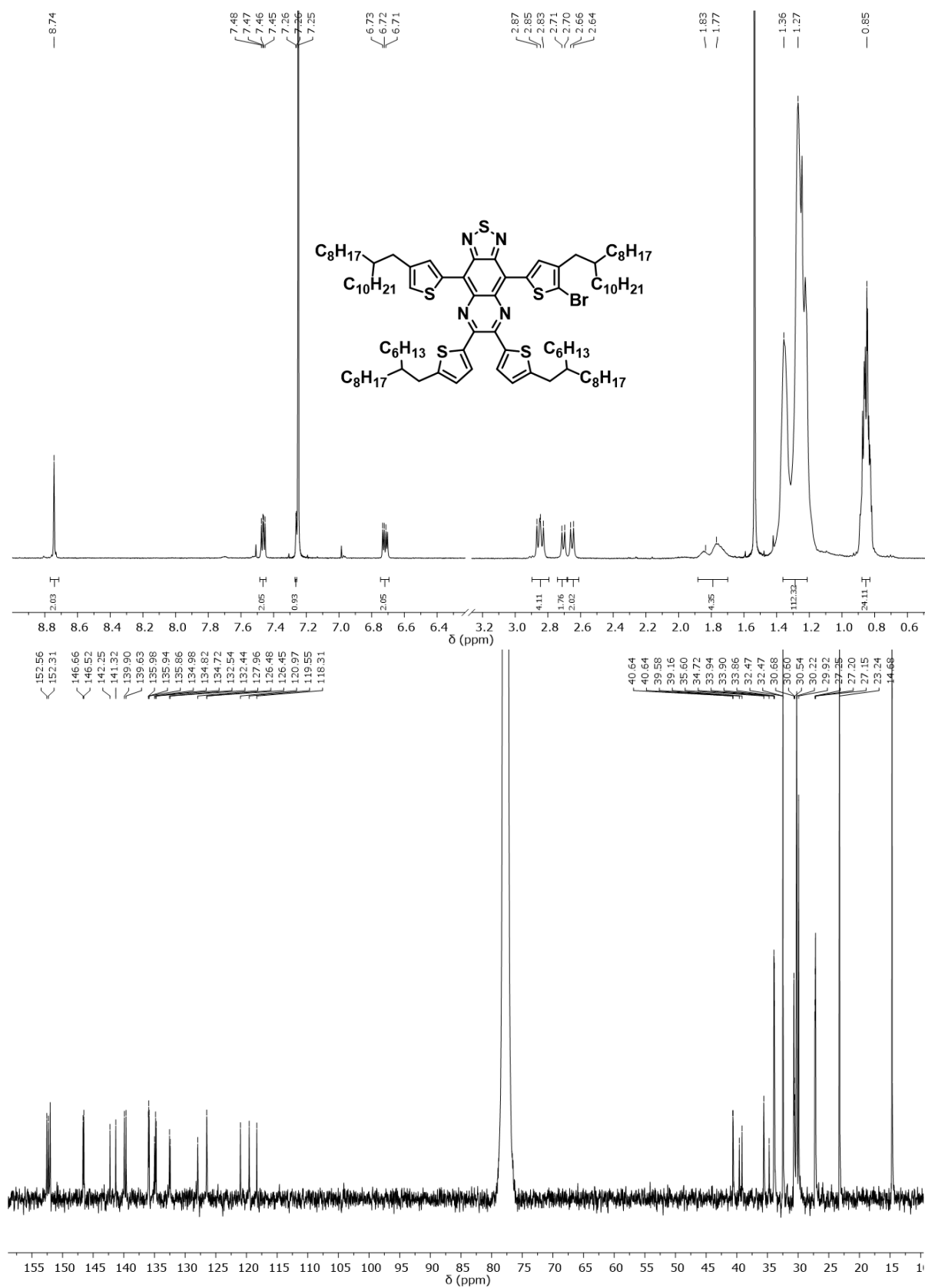


Figure S1: $^1\text{H-}$ and $^{13}\text{C-NMR}$ spectra of compound **13**.

4-(5-bromothiophen-2-yl)-6,7-bis(5-(2-hexyldecyl)thiophen-2-yl)-9-(thiophen-2-yl)-[1,2,5]thiadiazolo[3,4-g]quinoxaline (14)

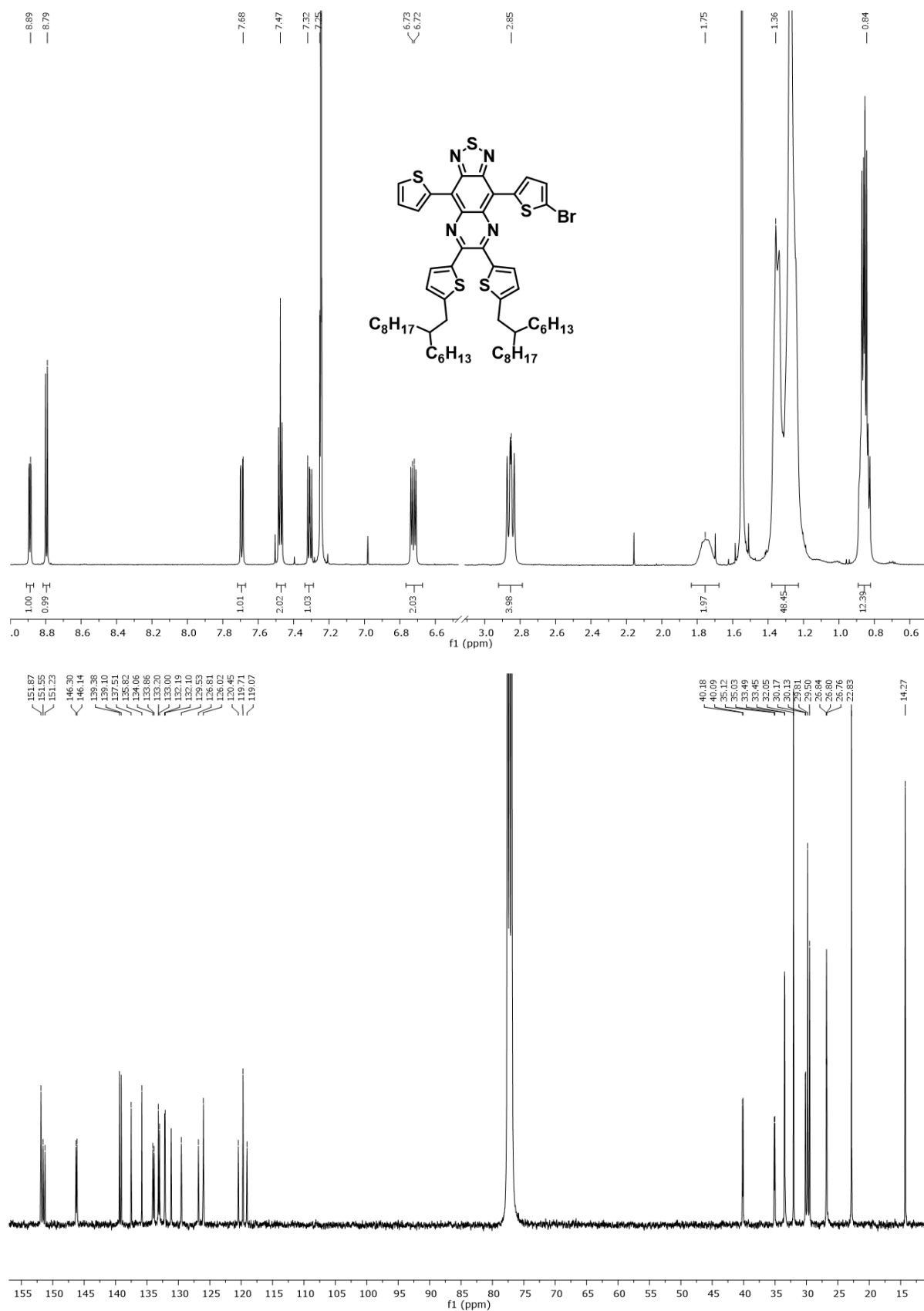


Figure S2: ¹H- and ¹³C-NMR spectra of compound 14.

4-(5-bromo-4-(2-octyldodecyl)thiophen-2-yl)-8-(4-(2-octyldodecyl)thiophen-2-yl)-1*H*,5*H*-benzo[1,2-*c*:4,5-*c'*]bis([1,2,5]thiadiazole) (15)

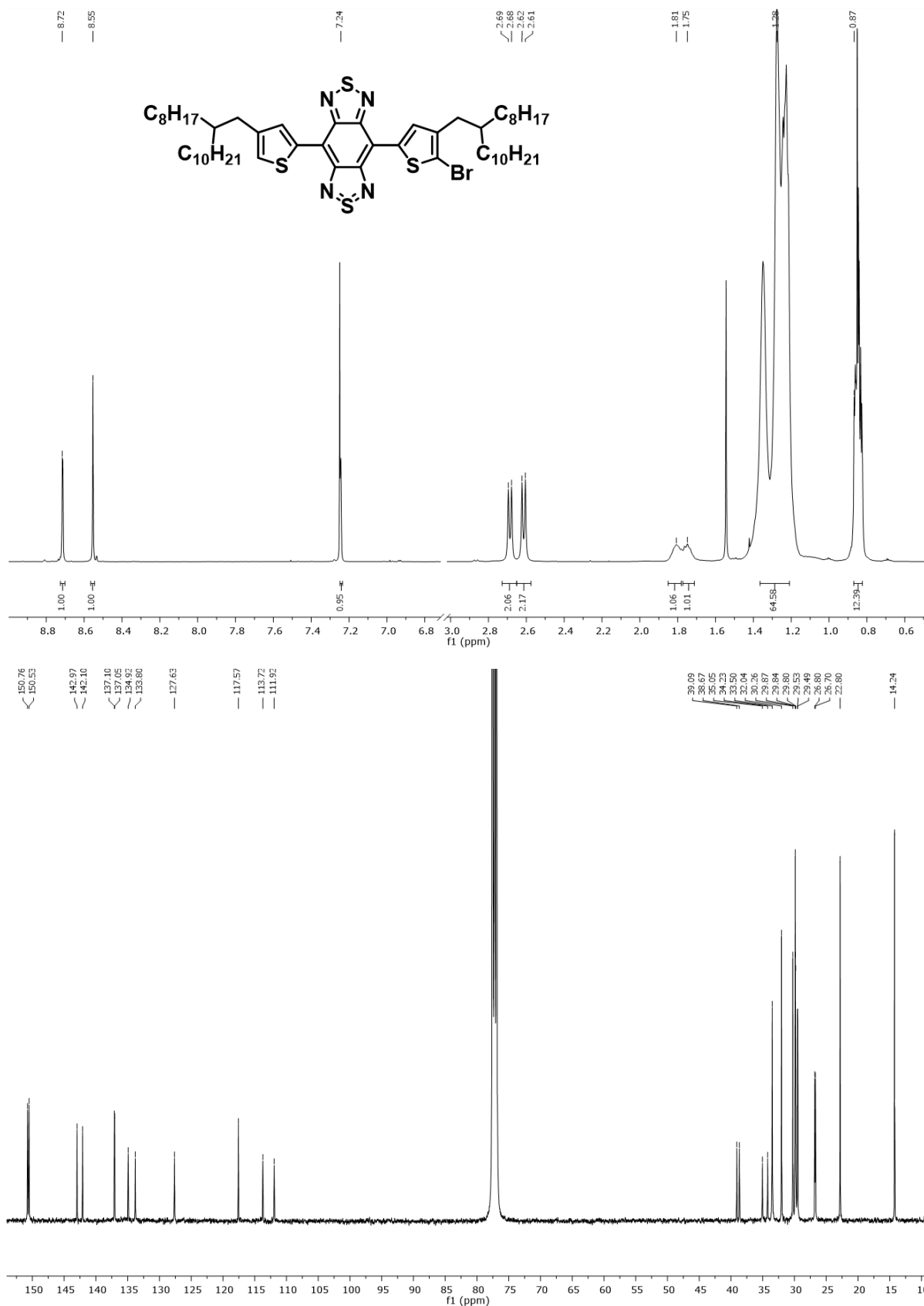


Figure S3: ¹H- and ¹³C-NMR spectra of compound 15.

5-(5-bromo-4-(2-octyldodecyl)thiophen-2-yl)-2,3-bis(5-(2-hexyldecyl)thiophen-2-yl)-7-(4-(2-octyldodecyl)thiophen-2-yl)thieno[3,4-*b*]pyrazine (16)

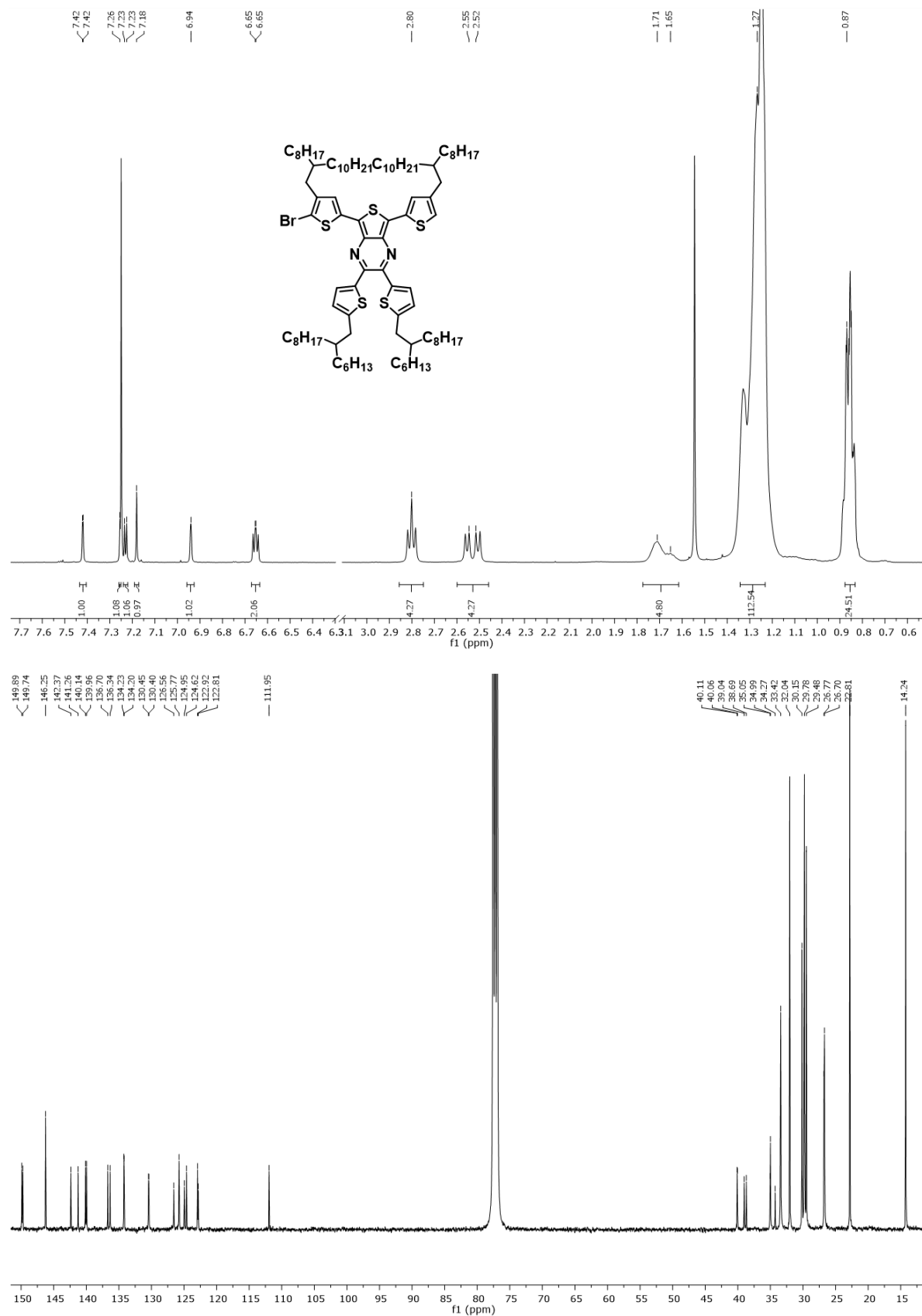


Figure S4: ¹H- and ¹³C-NMR spectra of compound 16.

R₂TQ-Por-TQR₂ (19)

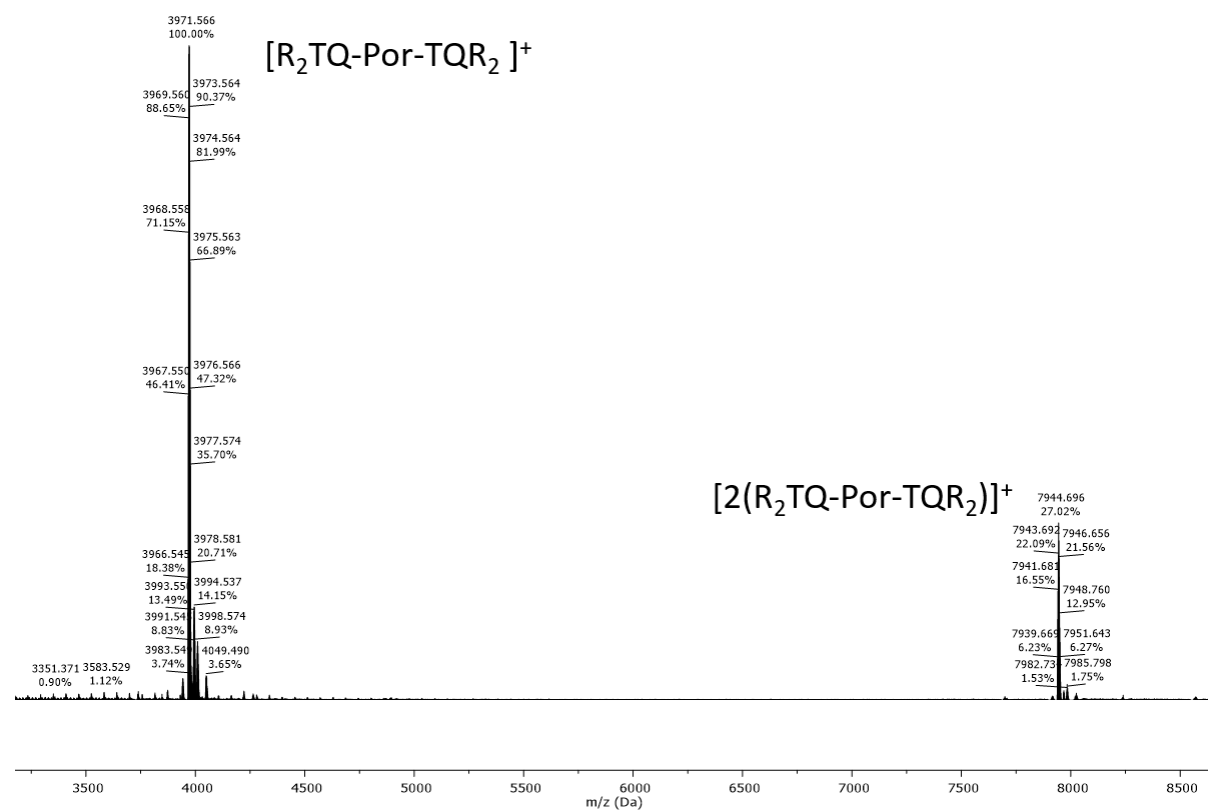
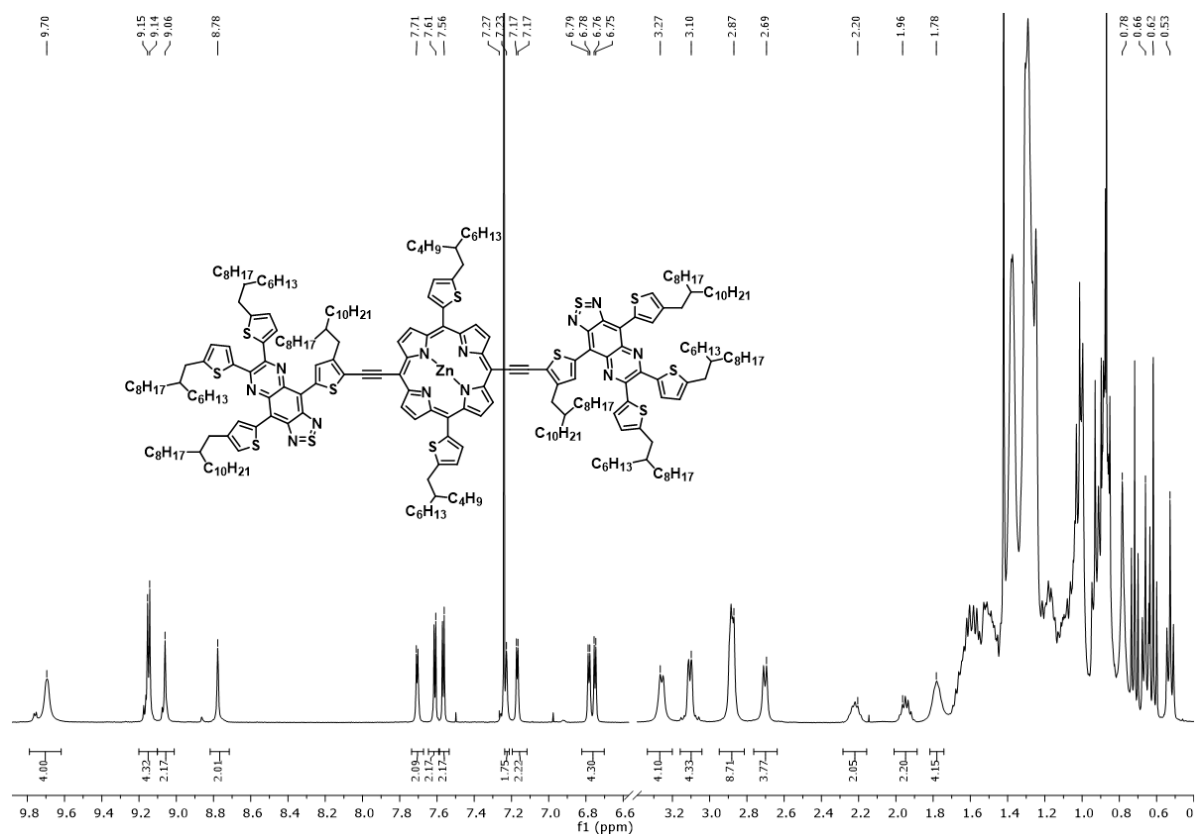


Figure S5: ¹H-NMR and MALDI-ToF mass spectra of compound 19.

TQ-Por-TQ (20)

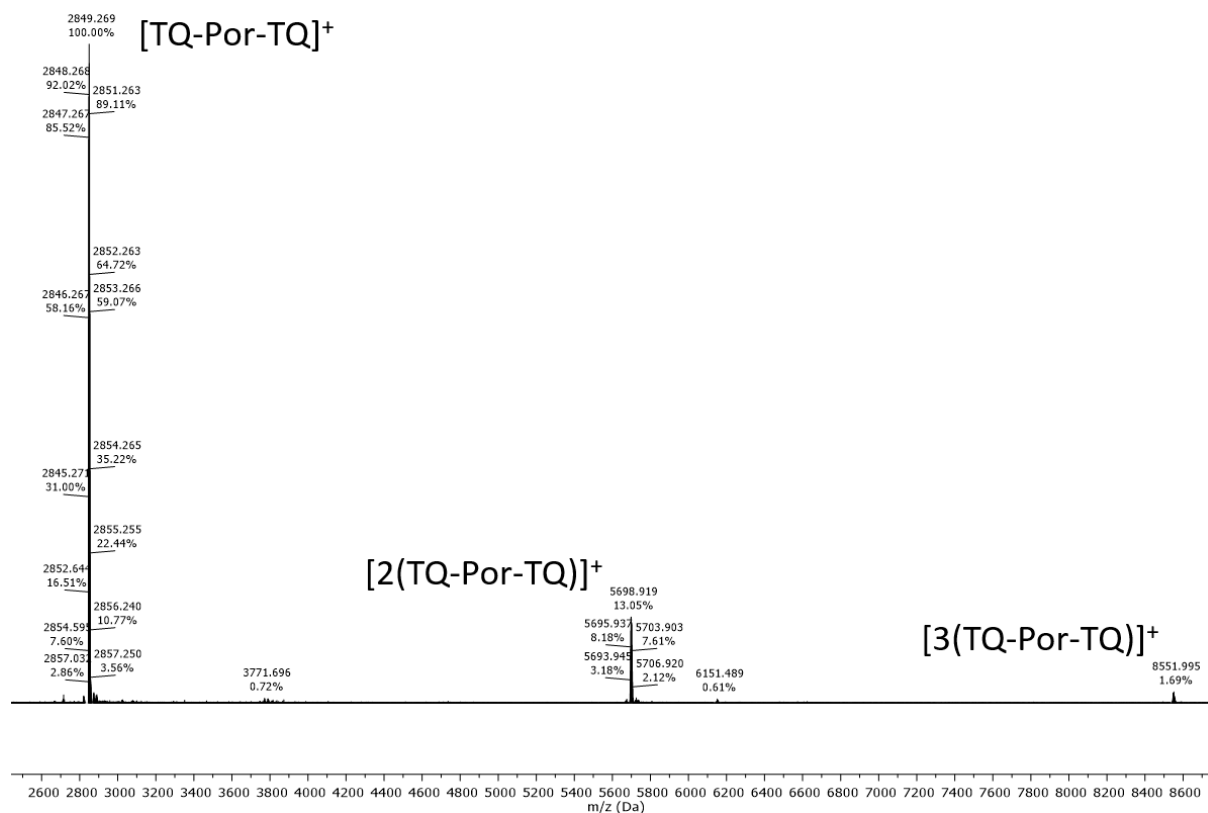
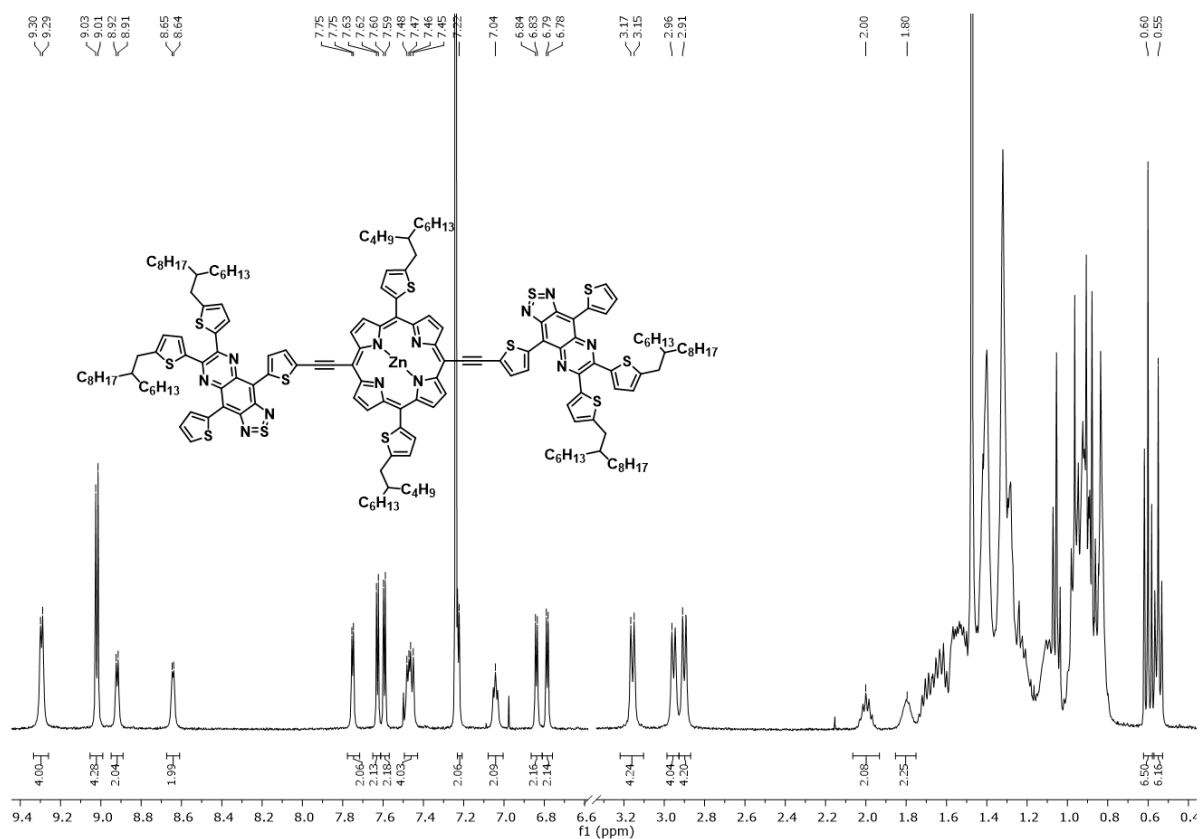


Figure S6: ¹H-NMR and MALDI-ToF mass spectra of compound 20.

BBT-Por-BBT (21)

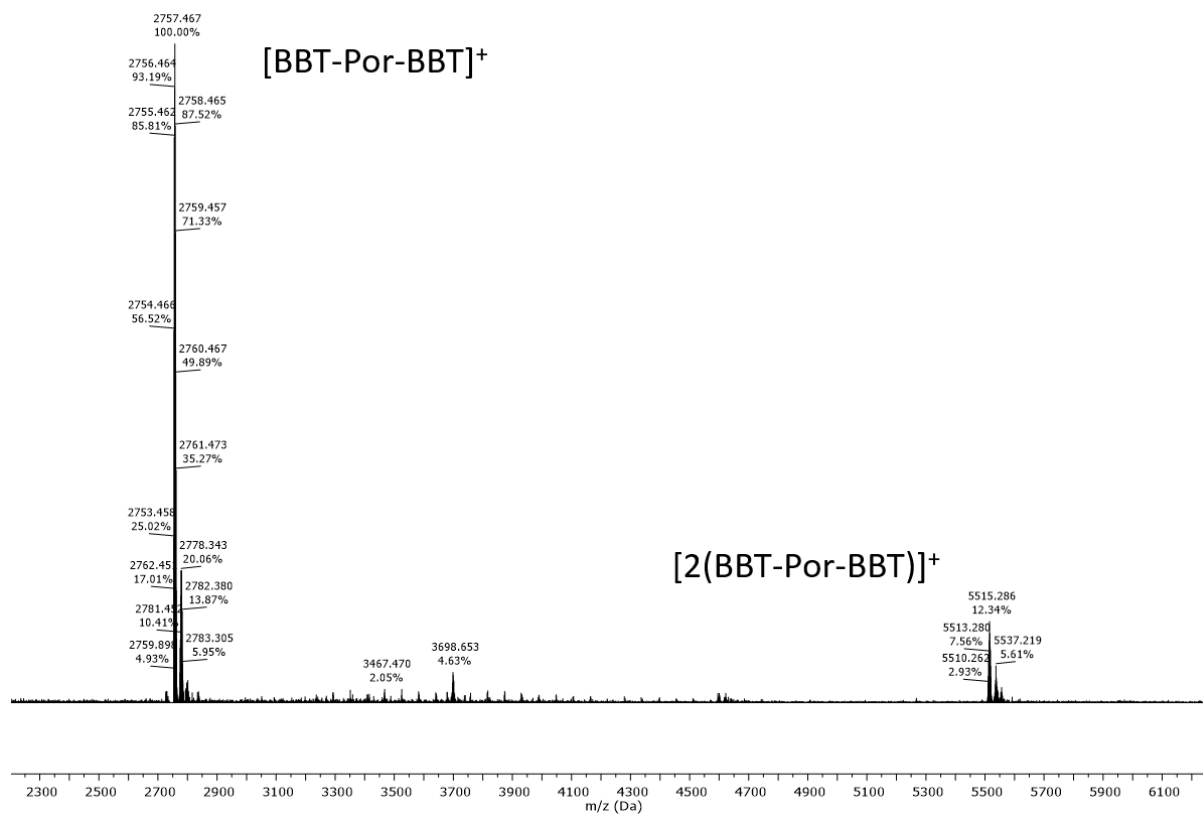
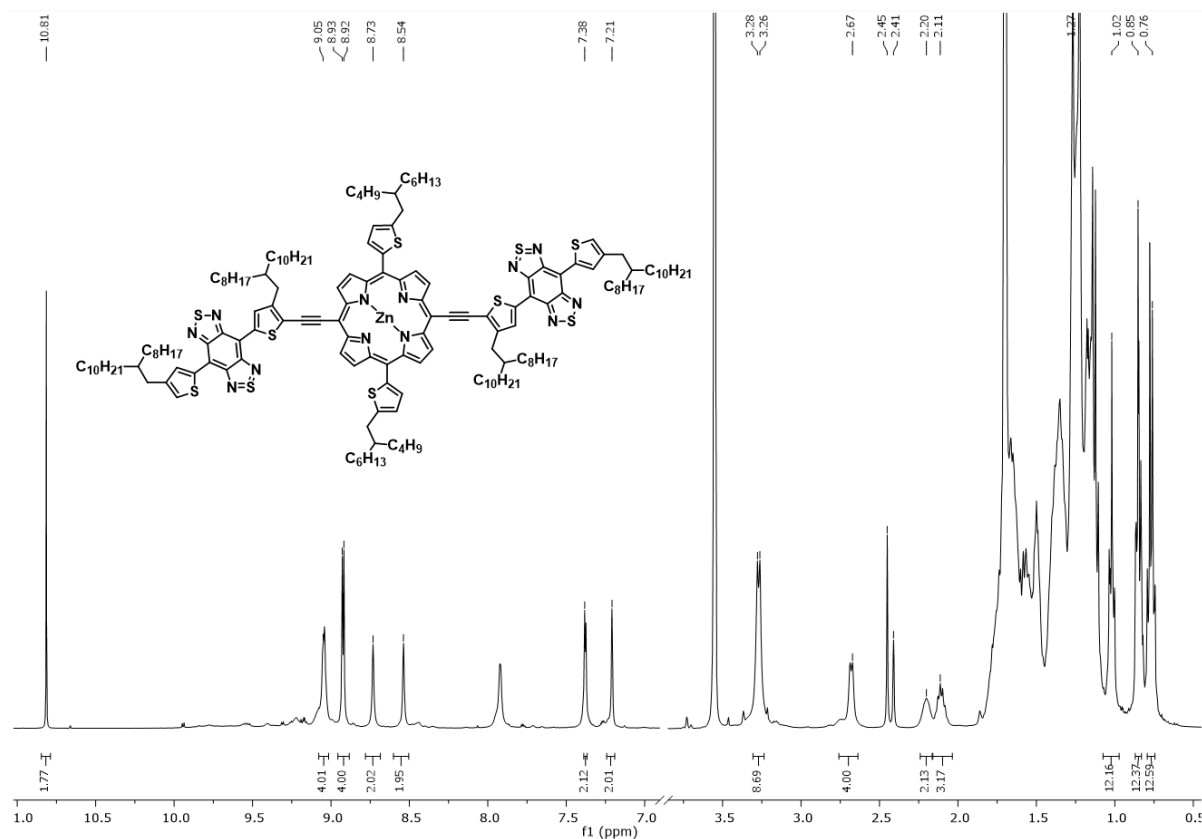


Figure S7: $^1\text{H-NMR}$ and MALDI-ToF mass spectra of compound **21**.

Por-TQ-Por (23)

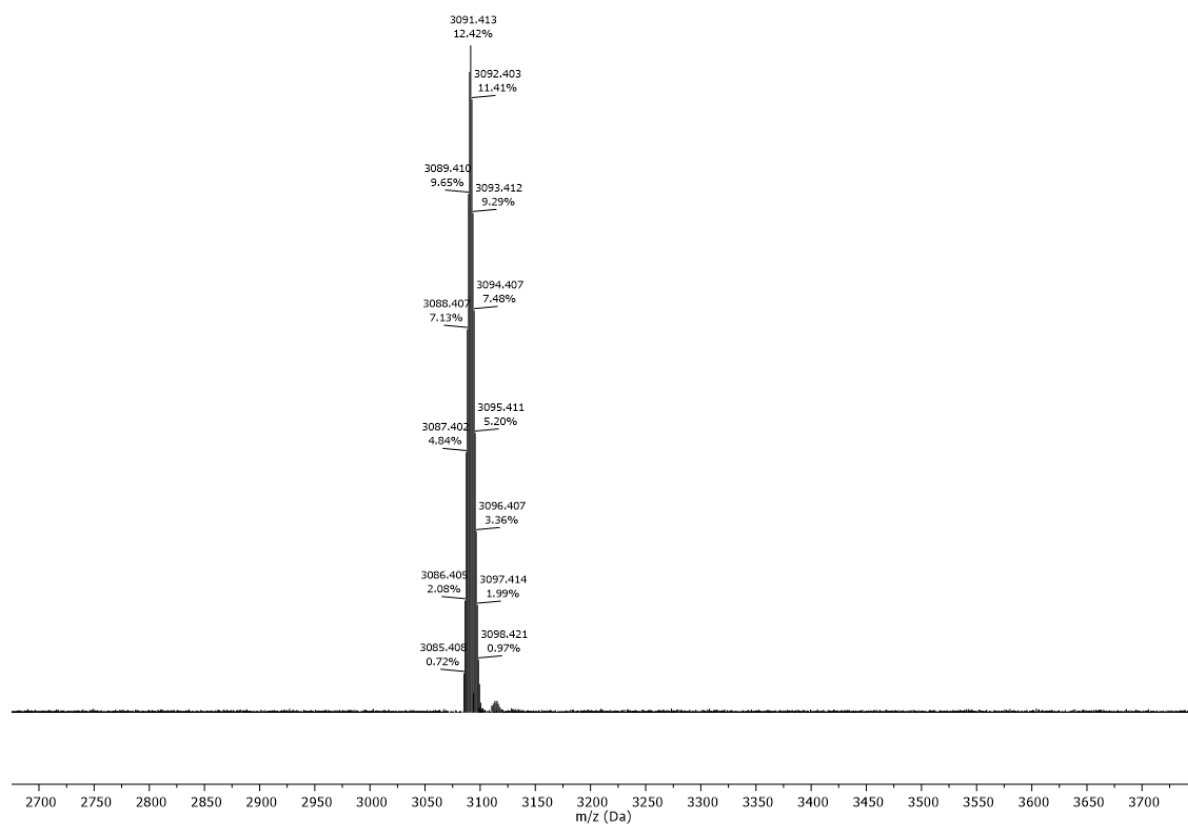
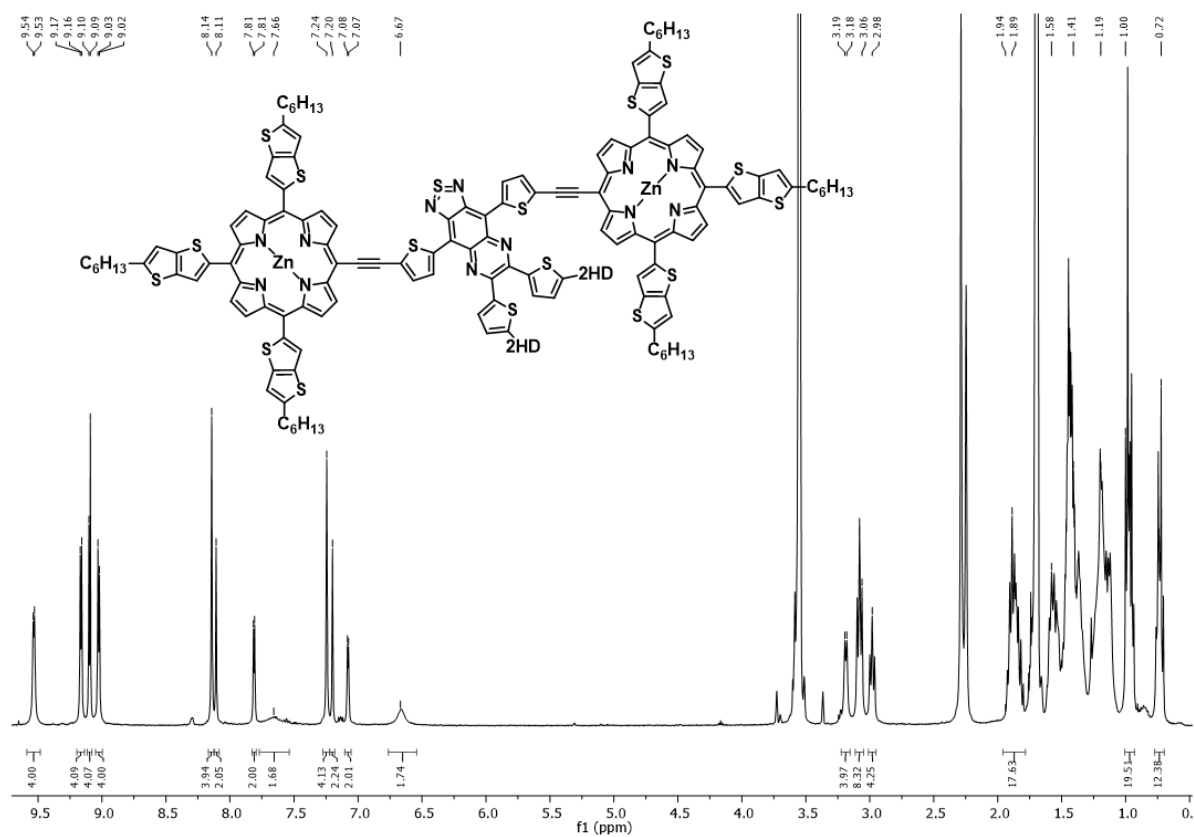


Figure S9: ¹H-NMR and MALDI-ToF mass spectra of compound **23**.

Por-TQ_n-Por (24)

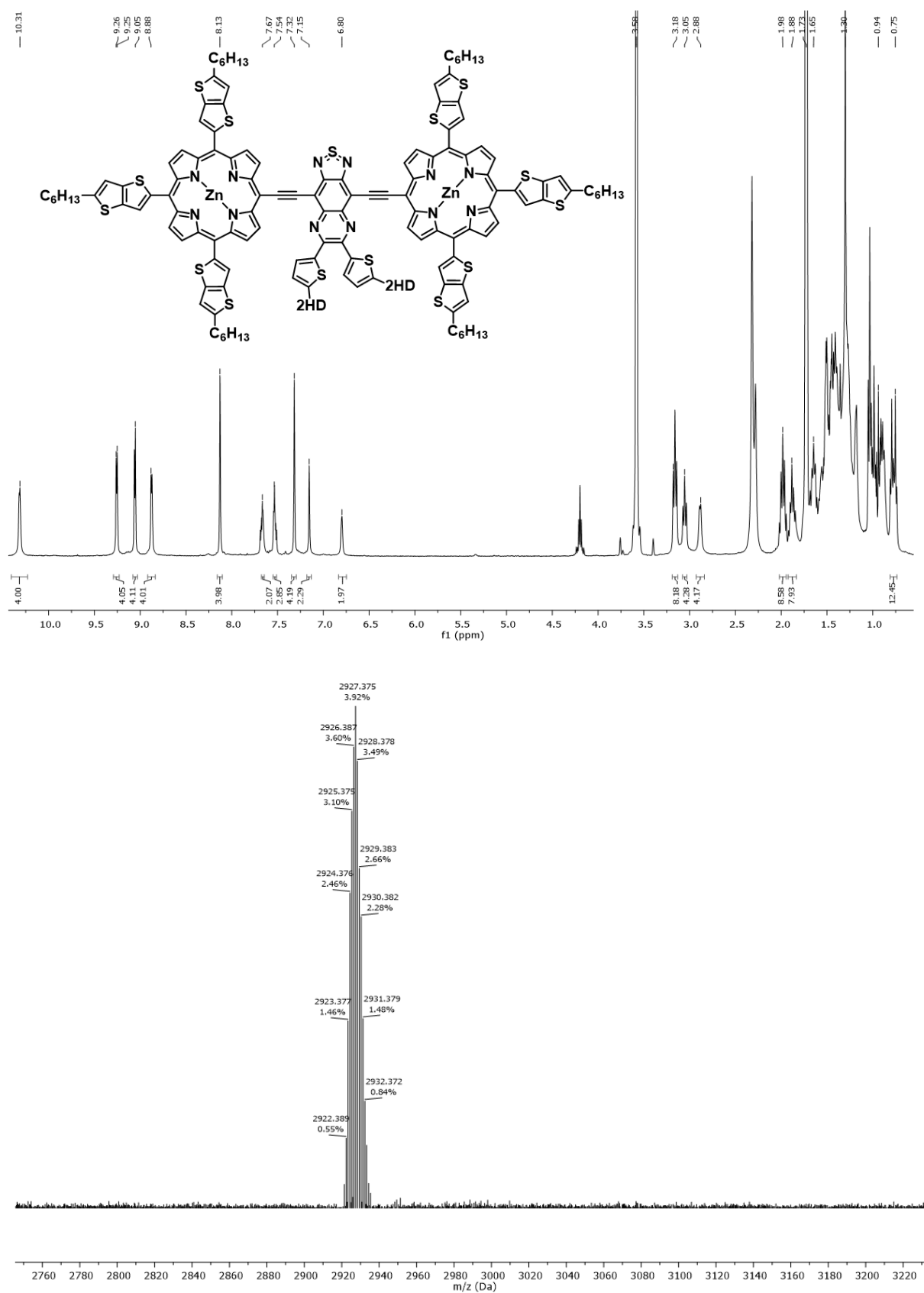


Figure S10: ¹H-NMR and MALDI-ToF mass spectra of compound 24.

1.4. UV-VIS-NIR absorption spectra

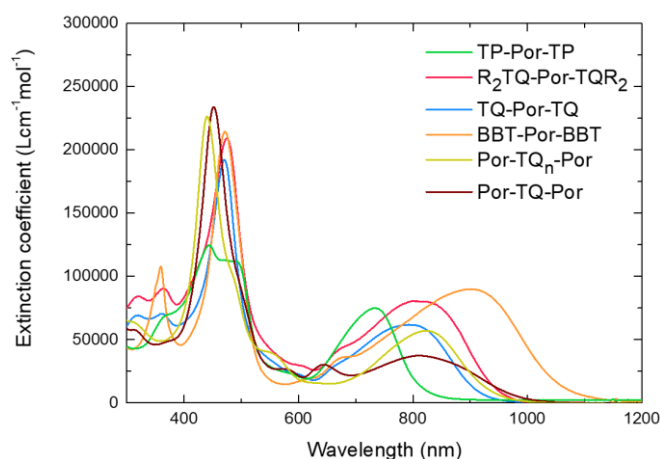


Figure S11: UV-VIS-NIR absorption spectra of the six final porphyrin materials in solution (CHCl_3).

1.5. Cyclic voltammetry

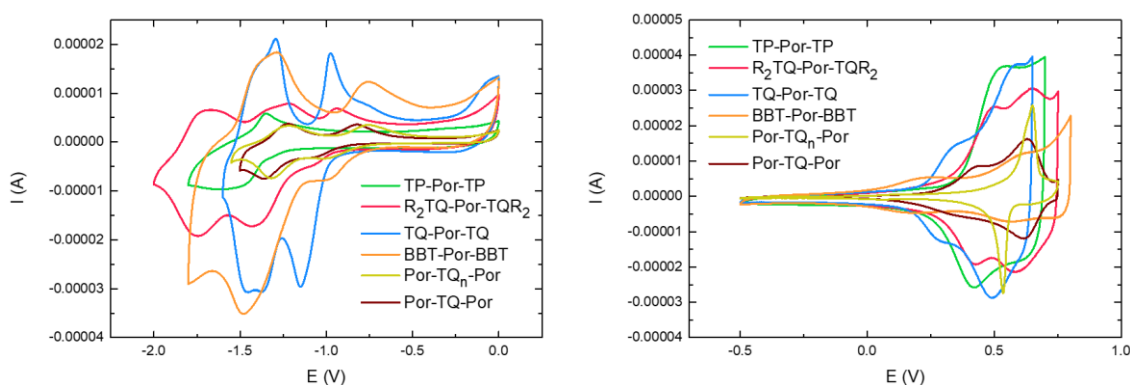


Figure S12: Reduction (left) and oxidation (right) traces for the CV measurements of the six final porphyrin materials (as films in $\text{MeCN-NBu}_4\text{PF}_6$).

Table S1: Optical and electrochemical properties of all meso-ethynyl-extended porphyrin chromophores.

compound	$\lambda_{\text{max VIS, film}}^{\text{a}}$ (nm)	$\lambda_{\text{max NIR, film}}^{\text{a}}$ (nm)	$E_{\text{red}}^{\text{b}}$ (V)	E_{ox}^{b} (V)	$E_{\text{LUMO}}^{\text{c}}$ (eV)	$E_{\text{HOMO}}^{\text{c}}$ (eV)	$E_{\text{g, opt}}^{\text{d}}$ (eV)
TP-Por-TP	494	786	-1.33	0.37	-3.58	-5.28	1.41
$\text{R}_2\text{TQ-Por-TQR}_2$	503	919	-0.98	0.48	-3.93	-5.39	1.22
TQ-Por-TQ	507	929	-0.99	0.22	-3.92	-5.13	1.20
BBT-Por-BBT	507	986	-0.87	0.05	-4.04	-4.96	1.09
Por-TQ _n -Por	457	873	-0.77	0.57	-4.13	-5.46	1.28
Por-TQ-Por	471	948	-0.87	0.29	-4.02	-5.19	1.14

^a Films were prepared by drop casting from chloroform onto a glass substrate. ^b Onset potentials vs Fc/Fc^+ . ^c Determined from the onset of oxidation/reduction in cyclic voltammetry. ^d Optical gap, determined from the onset of the solid-state VIS-NIR spectrum.

Section 2: Device characterization and optimization

2.1. Organic photodetector fabrication and characterization

Bulk heterojunction organic photodetectors were prepared using the inverted architecture glass/ITO/ZnO-PEIE/active layer/MoO₃/Ag. Prior to device processing, the ITO-coated glass substrates (100 nm, Ossila, sheet resistivity 20 Ω sq⁻¹) were thoroughly cleaned via sonication in soap water, demineralized water, acetone, and isopropanol, followed by a UV/O₃ treatment for 30 min. ZnO interlayers were spin-coated from a solution of Zn(OAc)₂·2H₂O (0.5 g, Merck) and ethanolamine (0.14 g, Merck) in 2-methoxyethanol (Merck). The ZnO layers were annealed at 300 °C for 10 min to obtain a layer thickness of ~30 nm. PEIE interlayers were spin-coated from a solution of PEIE (0.1 mL, 35–40 wt% in H₂O; Merck) in isopropanol (35 mL). Further processing was performed under nitrogen atmosphere in a glove box (<1 ppm O₂/H₂O). The photoactive layer solution, consisting of the photoactive porphyrin molecule and PC₇₁BM (>99%; Solenne), was then spin-coated according to the optimization protocol performed. The devices were prepared with a blend solution of 1:2 porphyrin:PC₇₁BM, with a total concentration of 36 mg mL⁻¹ in chloroform, chlorobenzene (CB), or *ortho*-dichlorobenzene (ODCB) and different amounts of pyridine or 1,8-diiodooctane as solvent additive. The solutions were stirred overnight at 60 °C to ensure complete dissolution. The active layer was deposited on top of the ZnO-PEIE layer by means of spin-coating at room temperature with an optimal layer thickness near 300 nm. Solvent vapor annealing was performed with different solvent (THF or CS₂) quantities (40, 60, and 80 μ L) and durations (15, 30, 60, and 120 s). Finally, the top electrodes MoO₃ (10 nm) and Ag (100 nm) were deposited by vacuum deposition to afford photodetector devices with an active area of 3 mm².

The *J-V* characteristics of all photodetectors in darkness were evaluated using a Keithley 2400 source meter. EQE measurements were performed using a homebuilt setup, combining a Newport Apex illuminator (100 W Quartz Tungsten Halogen lamp) as light source with a Newport Cornerstone 130° monochromator. The monochromated light was chopped at 123 Hz and the photocurrent was measured using a Stanford SR830 lock-in amplifier. A pyro-electric detector was employed as a reference cell.

AFM experiments were performed with a JPK NanoWizard 3 AFM (JPK Instruments AG, Berlin, Germany) using AC mode in air. Silicon ACTA-50 tips from AppNano with cantilever length ~125 μ m, spring constant ~40 N m⁻¹ and resonance frequency ~300 kHz were used. The scan angle, set point height, gain values and scan rate were adjusted according to the calibration of the AFM tip.

Grazing incidence wide angle X-ray scattering was performed at the Stanford Synchrotron Radiation Light source on beamline 11-3, with an X-ray energy of 12.7 keV and an incidence angle of 0.1°. The sample to detector distance was 317.3 mm and calibrated to a polycrystalline LaB6 standard.

Measurements were performed in a helium chamber to minimize air scattering. All data was corrected for the geometric distortion of the flat detector used, normalized by exposure time, sample thickness, monitor counts, and analyzed using Nika 1D SAXS1⁹ and WAXstools2 software in Igor Pro¹⁰.

Rise and fall time measurements were performed using a Thorlabs LED responding at 450 nm and driven by a Thorlabs LED high power driver DC2200. The photodetectors were connected to a Stanford Research Systems low-noise current preamplifier (model SR570) for which the signal was then sampled using an oscilloscope (model PicoScope 2000a).

2.2. Device optimization and characterization

At first, three different solvent systems were tested – chloroform, chlorobenzene (CB), and *ortho*-dichlorobenzene (ODCB) – for which the total concentration of **TQ-Por-TQ** and PC₇₁BM (36 mg/mL in a ratio of 1:2) was kept constant.⁴ From current-voltage (*I-V*) measurements, shown in Figure S13, it could be concluded that all three solvent systems produced similar dark current densities (J_D) near 200 nA/cm², open-circuit voltages (V_{OC}) near 0.6 V and light current densities (J_{ph} , under 1 sun irradiation) near 4 mA/cm² at -2 V. However, chloroform gave the most consistent results. Besides, investigation of the external quantum efficiency (EQE at 0 V and -2 V bias, Figure S13) revealed that the contribution in the NIR regime was highest for the devices prepared with chloroform as the casting solvent, reaching 7% and 15% at 900 nm at 0 and -2 V bias, respectively. The increased EQE in the visible part for the CB solvent system, for which PC₇₁BM is responsible, is of minor importance as NIR OPDs are targeted. Due to the small differences observed with respect to the processing solvent for the **TQ-Por-TQ** based device and the similarity of the **Por-TQ-Por** donor molecule with the earlier prepared D-A-D porphyrin molecules (all processed from CB),⁴ further solvent optimization was not performed on these valuable materials.

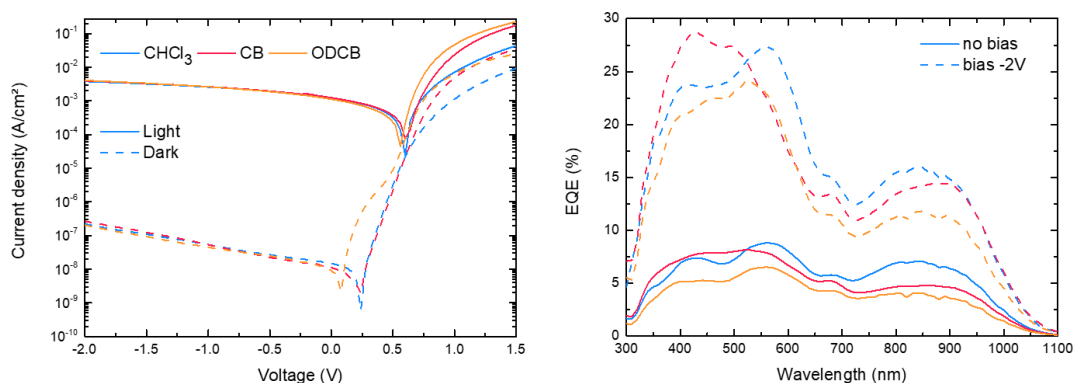


Figure S13: *J-V* curves and EQE spectra for the OPD devices based on the **TQ-Por-TQ:PC₇₁BM (1:2)** active layer blend as obtained during the solvent optimization process.

Both pyridine (Pyr) and 1,8-diiodooctane (DIO) were then used in various concentrations as solvent additives. Pyridine, known for its ability to coordinate to the zinc metal center of porphyrin molecules, reduces the stacking probability and possibly increases mixing with the fullerene acceptor.¹¹ DIO is a high-boiling solvent additive often used to control the active layer morphology in bulk heterojunctions.¹² Investigation of the J - V and EQE measurements of the **TQ-Por-TQ** based photodiodes (Figure S14) clarified that pyridine has a negative influence on both the light and dark current density and consequently on the EQE as well. However, a slight increase of the V_{OC} to 0.64 V was observed. Contrary, DIO had no significant influence on J_D . Only when 3 v/v% DIO was used, a slight increase was observed. In light conditions, DIO generally decreased the V_{OC} to 0.5 V and the J_{ph} to 1 mA/cm² at -2 V. An exception was observed for 1 v/v% DIO, for which J_{ph} was positively influenced, reaching a value of 5 mA/cm². Besides, a red-shift in the EQE spectrum was obtained, reaching 6 and 10% (at 0 and -2 V bias, respectively) at 1000 nm. This red-shift could be the result of a more optimized layer morphology with an increased stacking behavior of the porphyrin molecules. In case of **Por-TQ-Por**, the addition of DIO had a negative effect, generally resulting in shorted devices (Figure S15). Pyridine on the other hand decreased the V_{OC} from 0.60 to 0.44 V and produced a similar light and dark current density. A combination of Pyr and DIO (both in 1 v/v%) increased the light and dark current density by one order of magnitude accompanied with a slight V_{OC} decrease to 0.53 V. For this device an EQE of 2% and 7% (at 0 and -2 V bias, respectively) at 1000 nm was obtained. For all solvent systems and additive concentrations, different spin-coating speeds were tested, but no significant differences were obtained.

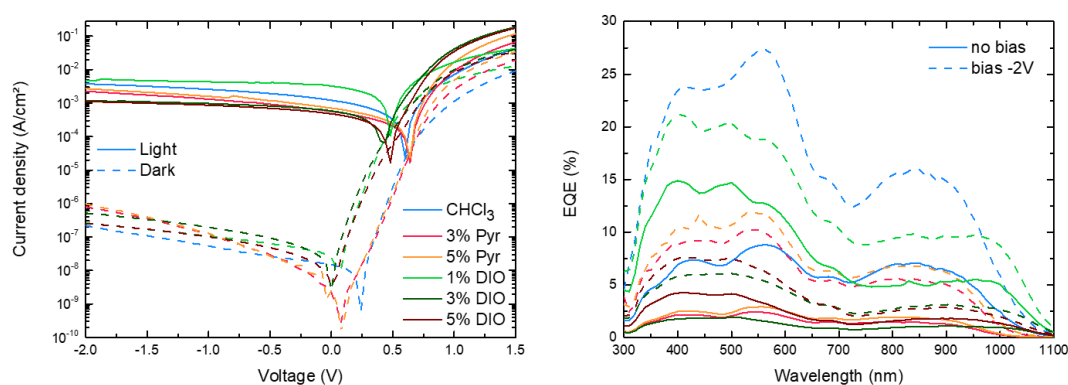


Figure S14: J - V curves and EQE spectra for the OPD devices based on the **TQ-Por-TQ:PC₇₁BM (1:2)** active layer blend as obtained during the solvent additive optimization process.

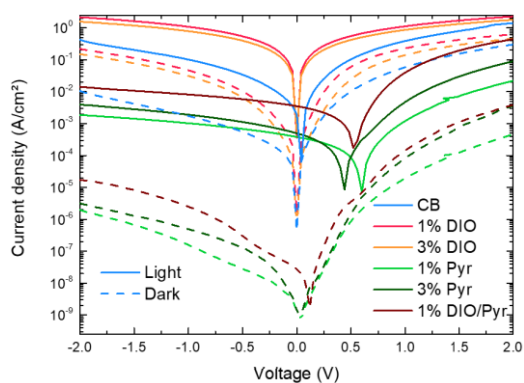


Figure S15: *J-V* curves for the OPD devices based on the **Por-TQ-Por**:PC₇₁BM (1:2) active layer blend as obtained during the solvent additive optimization process. EQEs are not really relevant due to shorted devices and very low J_{sc} values.

To further optimize the active layer morphology, solvent vapor annealing (SVA, setup shown in Figure S16) was applied. Variations in solvent quantity and SVA duration, shown in Table S2, positively influenced the V_{OC} and the fill factor (FF) for the **TQ-Por-TQ** based device when using THF as a solvent. A downside of the SVA strategy was observed for the J_D of the devices, generally increasing and becoming very inconsistent. EQE measurements also revealed an increased contribution of PC₇₁BM in the visible region. SVA on the **Por-TQ-Por** based devices was performed with three different solvents, i.e. THF, Pyr, and CS₂ (Table S3). The overall performance decreased by treating with either THF or Pyr vapor, but increased for CS₂.

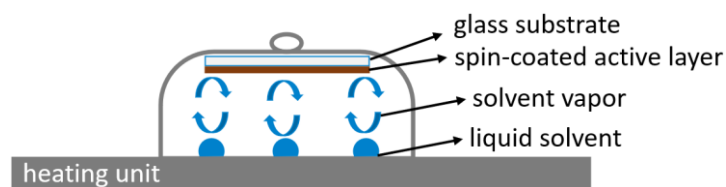


Figure S16: Solvent vapor annealing setup for post-fabrication modification of the active layer blend morphology.

Table S2: V_{OC} , J_{SC} , and FF values for the different conditions used during the solvent vapor annealing optimization for the **TQ-Por-TQ**:PC₇₁BM (1:2) photoactive layer blend. The solvent quantity (THF, in μL) and duration (in seconds) were varied.

reference		40 μL				60 μL			
		15'	30'	60'	120'	15'	30'	60'	120'
V_{OC} (V)	0.44	0.25	0.46	0.6	0.59	0.60	0.45	0.38	0.21
J_{SC} (mA/cm ²)	0.61	0.48	0.92	1.00	1.42	0.92	0.96	0.40	0.42
FF (%)	0.35	0.28	0.39	0.47	0.52	0.61	0.32	0.34	0.22
reference		80 μL							
		15'	30'	60'	120'				
V_{OC} (V)	0.44	0.5	0.52	0.30	0.38				
J_{SC} (mA/cm ²)	0.61	1.02	0.92	0.43	0.44				
FF (%)	0.35	0.68	0.42	0.31	0.30				

Table S3: V_{OC} , J_{SC} , and FF values for the different conditions used during the solvent vapor annealing optimization for the **Por-TQ-Por:PC₇₁BM (1:2)** photoactive layer blend. The solvent quantity (THF or CS₂, in μL) and duration (in seconds) were varied.

	reference CB 1% DIO, 1% Pyr	40 μL CS ₂			40 μL Pyr	40 μL THF
		30'	40'	50'	40'	40'
V_{OC} (V)	0.58	0.60	0.59	0.59	0.58	0.59
J_{SC} (mA/cm ²)	0.84	1.96	1.37	2.23	0.30	0.37
FF (%)	0.28	0.33	0.29	0.33	0.29	0.29

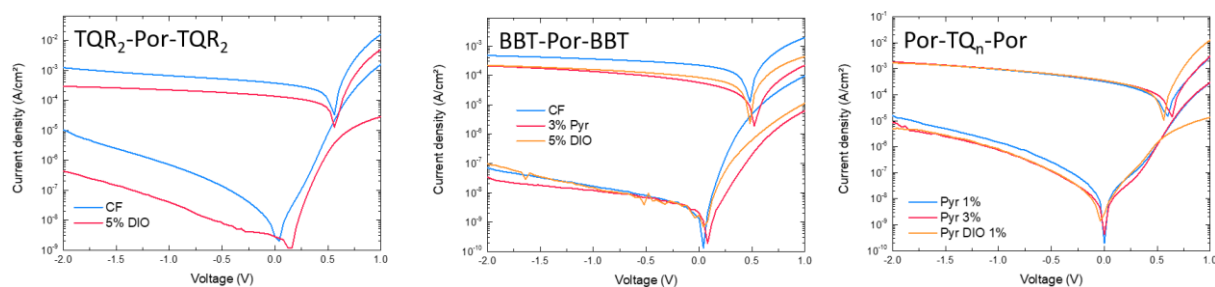


Figure S17: J-V (single device) data for the **R₂TQ-Por-TQR₂**, **BBT-Por-BBT**, and **Por-TQ_n-Por** based OPD devices (blends with PC₇₁BM in a 1:2 ratio).

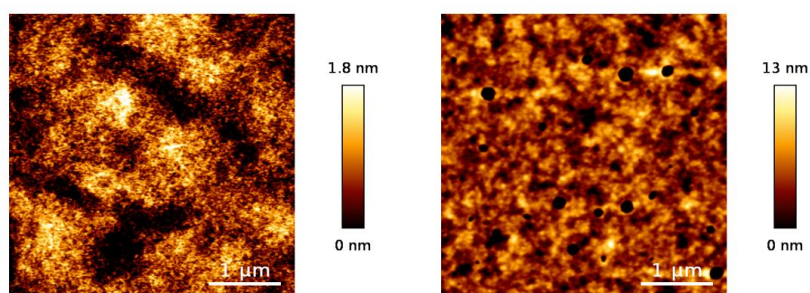


Figure S18: AFM images for the optimized **TQ-Por-TQ:PC₇₁BM** based OPD device (left, deposition from CHCl₃ without additive or SVA) and for the optimized **Por-TQ-Por:PC₇₁BM** based OPD device (right, deposition from chlorobenzene with 1 v/v% DIO and Pyr and SVA with CS₂).

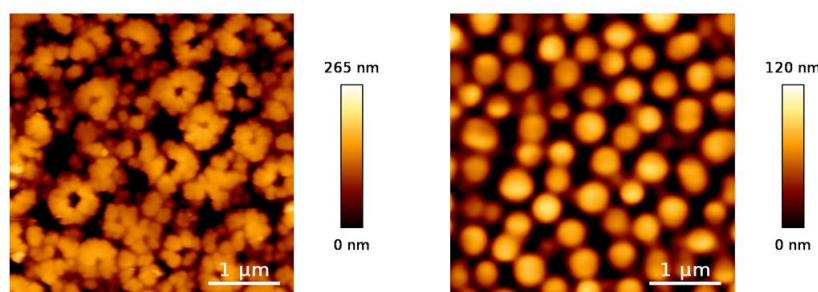


Figure S19: AFM images for the **R₂TQ-Por-TQR₂** (left, deposition from CHCl₃) and **BBT-Por-BBT** based blends with PC₇₁BM (right, deposition from CHCl₃).

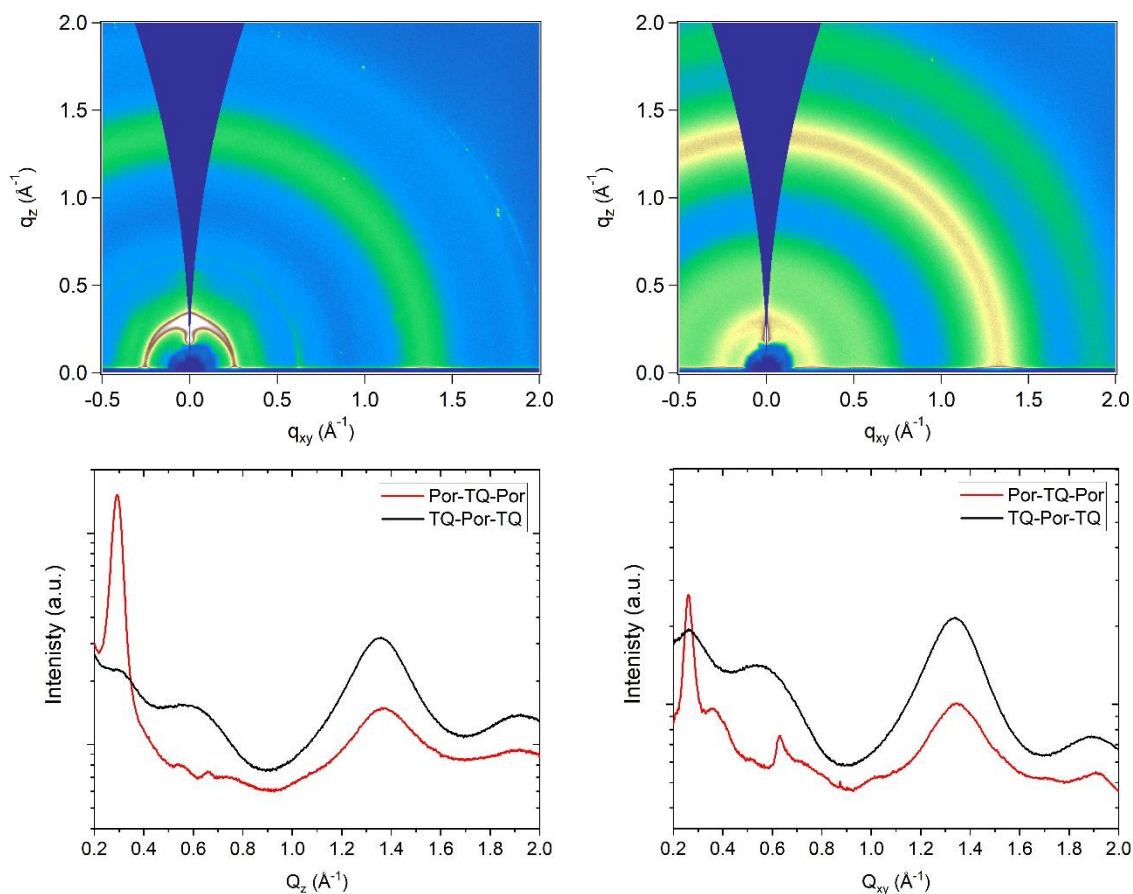


Figure S20: 2D-GIWAXS patterns for **Por-TQ-Por** (top left) and **TQ-Por-TQ** (top right) blended in a 1:2 ratio with $PC_{71}BM$ and line profiles in the Q_z (bottom left) and Q_{xy} (bottom right) scattering directions. The sharp lamellar stacking peak in **Por-TQ-Por** suggests ordered packing of crystallites, whereas the larger fraction of branched 2-hexyldecyl side chains on the **TQ-Por-TQ** moiety appears to introduce disorder along the lamellar direction. Note that the intensity scales of the 2D images are identical for comparison.

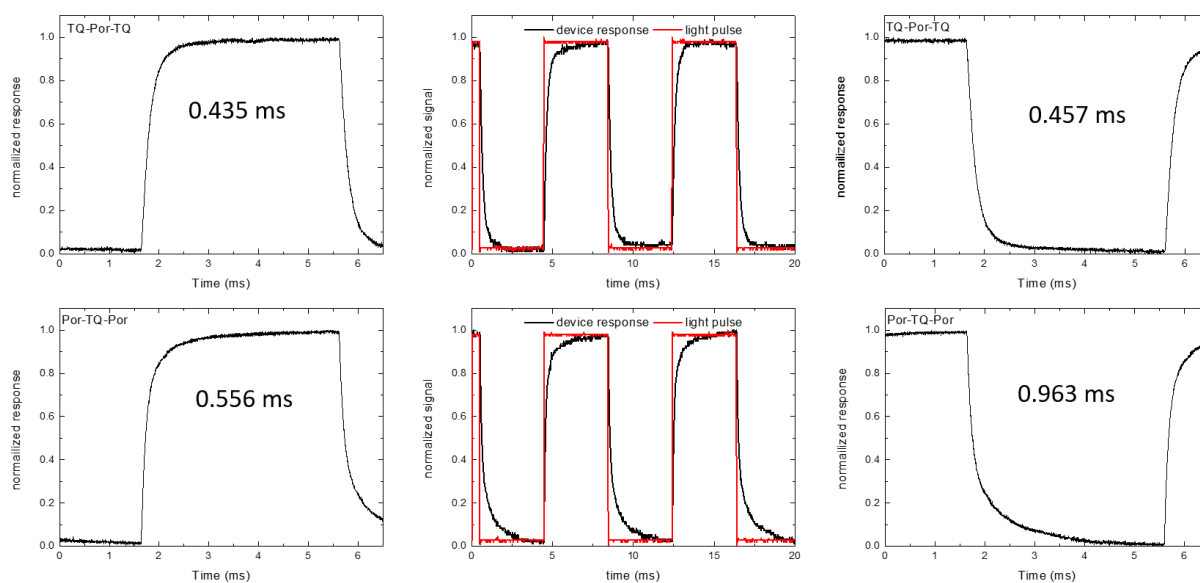


Figure S21: Rise (left) and fall (right) times for the optimized *TQ-Por-TQ* (top) and *Por-TQ-Por* (bottom) based OPD devices. The middle graphs show the light pulse train and device response on a 20 ms time interval.

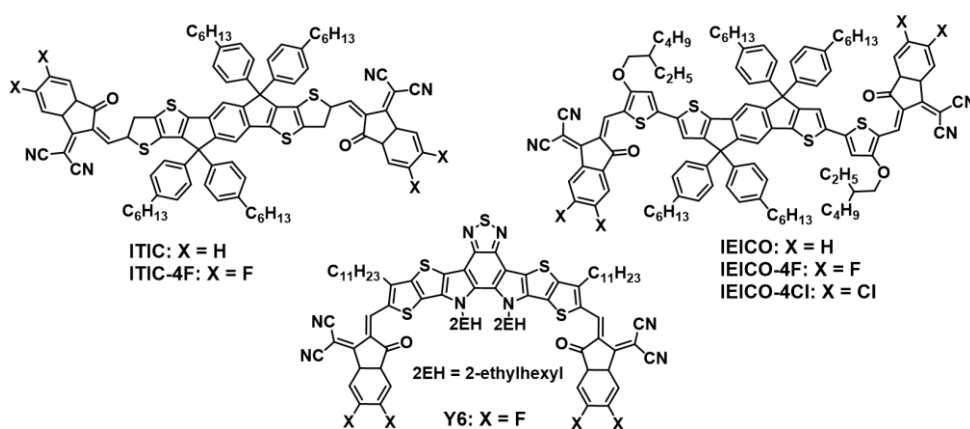


Figure S22: Chemical structures of selected NFAs.

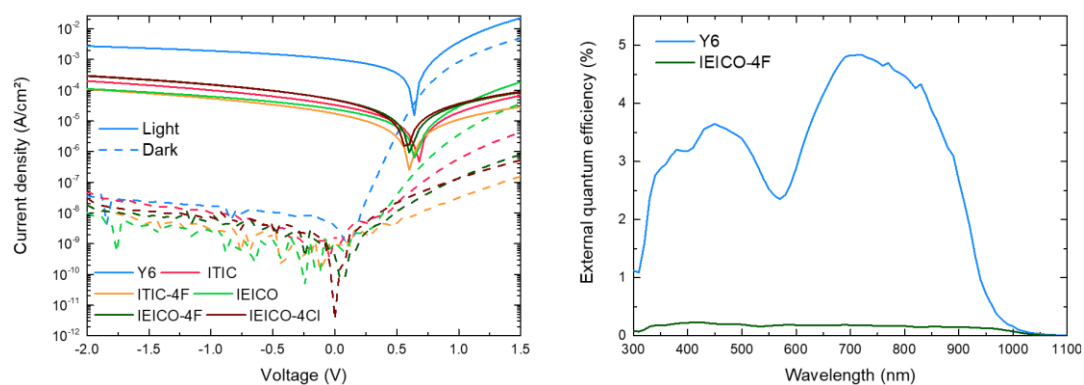


Figure S23: J-V curves and EQE spectra for the NFA optimization process (using *TQ-Por-TQ* as the donor). EQE spectra of several active layers were too noisy to allow an accurate measurement.

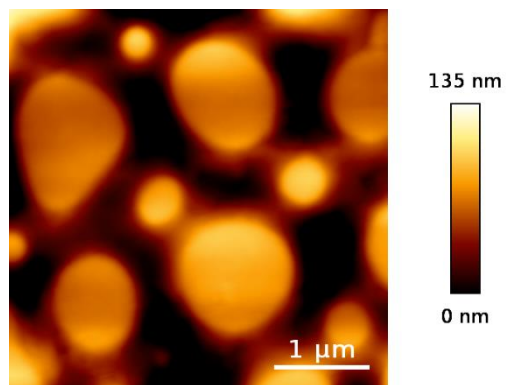


Figure S24: AFM image of the *TQ-Por-TQ:Y6* blend.

Section 3: Synthesis and characterization of the precursors for strategy 2 and TII-Por-TII

3.1. Materials and methods

See section 1.1.

3.2. Synthesis and characterization of the precursors, the ethynyl-extended acceptor chromophores, and TII-Por-TII

All reagents and chemicals were obtained from commercial sources and used without further purification. Solvents were dried on a solvent purification system (MBraun, MB-SPS-800) equipped with alumina columns. All acceptor molecule cores were prepared via literature procedures; TII (thienoisindigo),¹³ TQ (thiadiazolo[3,4-*g*]quinoxaline),⁷ TP (thieno[3,4-*b*]pyrazine),¹⁴ BBT (benzobisthiadiazole),¹⁵ and TTD (thienothiadiazole).¹⁴ Monobromination and the consecutive Sonogashira cross-coupling were performed via standard procedures explained below.

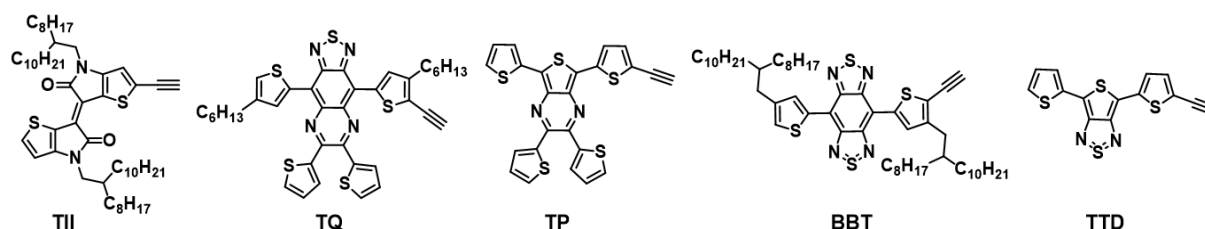
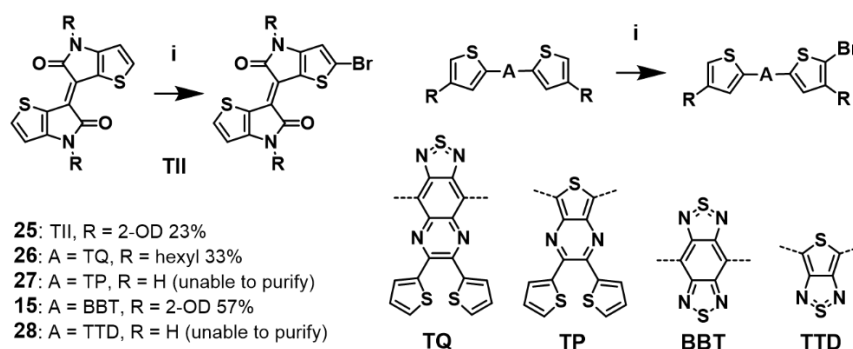


Figure S25: Overview of the intended acceptor molecules for the alternative Sonogashira cross-coupling reaction (strategy 2) on dibrominated A_2B_2 -porphyrin precursor **7**.

General monobromination procedure: The acceptor material was dissolved in $CHCl_3$ and the solution was cooled down to 0 °C while stirring. Then, NBS (1 equiv.) was added portionwise and the mixture was stirred overnight, slowly heating up to room temperature. The solvents were removed and column chromatography (silica, $CHCl_3$:petroleum ether mixture) was performed to yield the pure product.



Scheme S7: Monobromination of the acceptor molecules: *i*) NBS (1 equiv), $CHCl_3$, RT.

(E)-2-bromo-4,4'-bis(2-octyldodecyl)-[6,6'-bithieno[3,2-*b*]pyrrolylidene]-5,5'(4*H*,4'*H*)-dione (25).

Column chromatography (CH_2Cl_2 :petroleum ether, 30:70) was performed to yield the pure product as

a purple oil. Yield = 23% (149 mg). $^1\text{H-NMR}$ (400 MHz, CDCl_3), δ (ppm): 7.54 (d, $J = 5.2$ Hz, 1H), 6.81 (s, 1H), 6.76 (d, $J = 5.2$ Hz, 1H), 3.66 (d, $J = 7.4$ Hz, 2H), 3.63 (d, $J = 7.4$ Hz, 2H), 1.90–1.80 (br, 2H), 1.40–1.18 (br, 64H), 0.88–0.83 (m, 12H).

4-(5-bromo-4-hexylthiophen-2-yl)-9-(4-hexylthiophen-2-yl)-6,7-di(thiophen-2-yl)-

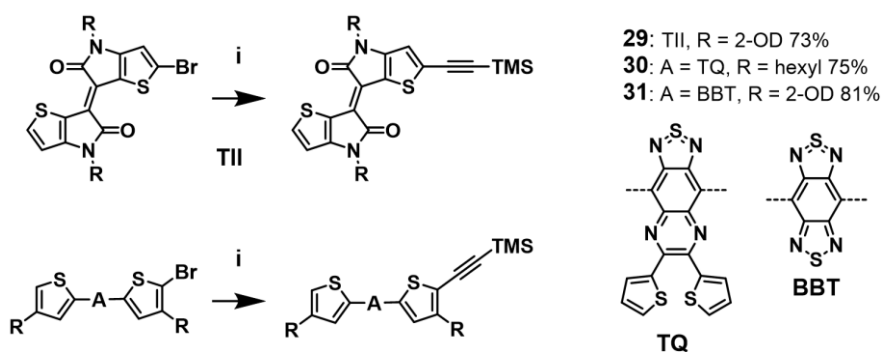
[1,2,5]thiadiazolo[3,4-*g*]quinoxaline (26). Column chromatography (CHCl_3 :petroleum ether, 5:95) was performed to yield the pure product as a purple solid. Yield = 33% (180 mg). $^1\text{H-NMR}$ (400 MHz, CDCl_3), δ (ppm): 8.75 (s, 1H), 8.74 (d, $J = 1.2$ Hz, 1H), 7.66 (dd, $J = 5.0, 1.0$ Hz, 1H), 7.60 (dd, $J = 5.0, 1.0$ Hz, 1H), 7.55 (dd, $J = 3.8, 1.0$ Hz, 1H), 7.53 (dd, $J = 3.8, 1.0$ Hz, 1H), 7.32 (d, $J = 1.1$ Hz, 1H), 7.10–7.05 (m, 2H), 2.77 (t, $J = 7.6$ Hz, 2H), 2.72 (t, $J = 7.6$ Hz, 2H), 1.80–1.70 (m, 4H), 1.47–1.32 (m, 12H), 0.90 (t, $J = 7.1$ Hz, 6H).

5-(5-bromothiophen-2-yl)-2,3,7-tri(thiophen-2-yl)thieno[3,4-*b*]pyrazine (27). The crude product was a mixture of starting material, mono- and dibrominated product. Column chromatography (CHCl_3 :petroleum ether, 5:95) was performed. However, due to the limited solubility, the monobrominated product could not be completely purified.

4-(5-bromo-4-(2-octyldodecyl)thiophen-2-yl)-8-bis(4-(2-octyldodecyl)thiophen-2-yl)-1*H*,5*H*-benzo[1,2-*c*:4,5-*c'*]bis([1,2,5]thiadiazole) (15). See section 1.

4-(5-bromothiophen-2-yl)-6-(thiophen-2-yl)-1*H*,3*H*-thieno[3,4-*c*][1,2,5]thiadiazole (28). The crude product was a mixture of starting material, mono- and dibrominated product. Column chromatography (CHCl_3 :petroleum ether, 25:75) was performed. However, due to the limited solubility, the monobrominated product could not be completely purified.

Sonogashira cross-coupling procedure for the monofunctionalized acceptor materials: The monobrominated acceptor **15**, **25**, or **26** (1 equiv.) and trimethylsilylacetylene (5 equiv.) were placed in a Schlenk flask and flushed three times with N_2 , after which dry THF (7.3 mM) and dry Et_3N (3.7 mM) were added. Then, the mixture was purged with N_2 for 30 min. Afterwards, $\text{Pd}(\text{PPh}_3)_2\text{Cl}_2$ (0.05 equiv.) and CuI (0.05 equiv.) were added and the reaction was stirred overnight. Next morning, the reaction mixture was cooled down, water was added and extraction was done with CHCl_3 . The organic solution was dried over MgSO_4 , filtered and evaporated to dryness. Flash column chromatography (silica) was performed, yielding the pure product.



Scheme S8: Sonogashira cross-coupling for the alkylation of the monofunctionalized acceptor molecules: i) TMS-acetylene, Pd(PPh₃)₂Cl₂, CuI, Et₃N, THF, RT.

(E)-4,4'-bis(2-octyldodecyl)-2-((trimethylsilyl)ethynyl)-[6,6'-bithieno[3,2-b]pyrrolylidene]-

5,5'(4H,4'H)-dione (29). Column chromatography (CHCl₃:petroleum ether, 30:70) was performed to yield the pure product as a green solid. Yield = 73% (111 mg). ¹H-NMR (400 MHz, CDCl₃), δ(ppm): 7.53 (d, *J* = 5.2 Hz, 1H), 6.84 (s, 1H), 6.76 (d, *J* = 5.2 Hz, 1H), 3.66 (d, *J* = 7.6 Hz, 2H), 3.63 (d, *J* = 7.6 Hz, 2H), 1.90–1.80 (br, 2H) 1.40–1.18 (br, 64H), 0.89–0.82 (m, 12H), 0.25 (s, 9H).

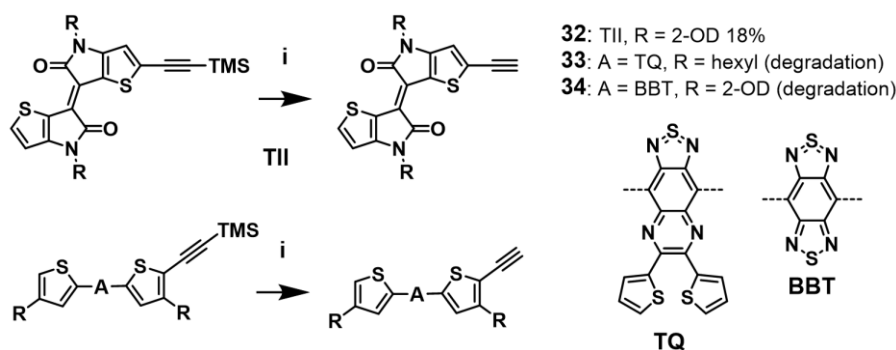
4-(4-hexyl-5-((trimethylsilyl)ethynyl)thiophen-2-yl)-9-(4-hexylthiophen-2-yl)-6,7-di(thiophen-2-yl)[1,2,5]thiadiazolo[3,4-g]quinoxaline (30).

Column chromatography (CHCl₃:petroleum ether, 40:60) was performed to yield the pure product as a purple solid. Yield = 75% (138 mg). ¹H-NMR (400 MHz, CDCl₃), δ(ppm): 8.73 (s, 1H), 8.70 (d, *J* = 1.3 Hz, 1H), 7.62 (dd, *J* = 5.0, 1.0 Hz, 1H), 7.59 (dd, *J* = 5.0, 1.0 Hz, 1H), 7.53 (dd, *J* = 3.8, 1.0 Hz, 1H), 7.51 (dd, *J* = 3.8, 1.0 Hz, 1H), 7.27 (d, *J* = 1.3 Hz, 1H), 7.08–7.04 (m, 2H), 2.82 (t, *J* = 7.6 Hz, 2H), 2.75 (t, *J* = 7.6 Hz, 2H), 1.81–1.71 (m, 4H), 1.48–1.30 (m, 12H), 0.91 (t, *J* = 7.2 Hz, 6H), 0.31 (s, 9H).

4-(4-(2-octyldodecyl)-5-((trimethylsilyl)ethynyl)thiophen-2-yl)-8-(4-(2-octyldodecyl)thiophen-2-yl)-1H,5H-benzo[1,2-c:4,5-c']bis([1,2,5]thiadiazole) (31).

Column chromatography (hexanes:CHCl₃, 65:35) was performed to yield the pure product as a green solid. Yield = 81% (105 mg). ¹H-NMR (400 MHz, CDCl₃): δ (ppm) = 8.83 (d, *J* = 1.0 Hz, 1H), 8.80 (s, 1H), 7.28 (d, *J* = 1.0 Hz, 1H), 2.75 (d, *J* = 7.0 Hz, 2H), 2.70 (d, *J* = 6.8 Hz, 2H), 1.89–1.81 (br, 1H), 1.78–1.70 (br, 1H), 1.40–1.20 (m, 64H), 0.87–0.81 (m, 12H), 0.28 (s, 9H).

General TMS deprotection procedure for the monofunctionalized acceptor materials: The acceptor molecule **29**, **30**, or **31** (1 equiv.) was dissolved in THF (0.003 M) and the solution was cooled down to 0 °C. Then, a solution of KOH (1.5 equiv.) in H₂O (0.03 M) was added and the mixture was stirred for 30 min. Afterwards, the reaction was continued for 2.5 h at room temperature. Upon completion, the reaction mixture was cooled down, water was added and extraction was done with CHCl₃. The organic solution was dried over MgSO₄, filtered and evaporated to dryness. Finally, flash column chromatography (silica) was performed.



Scheme S9: TMS deprotection of the monofunctionalized acceptor molecules: i) KOH (aq.), THF, RT.

(E)-2-ethynyl-4,4'-bis(2-octyldodecyl)-[6,6'-bithieno[3,2-b]pyrrolylidene]-5,5'(4H,4'H)-dione (32).

Column chromatography (CHCl₃:hexanes, 50:50) was performed to yield the pure product as a purple solid. Yield = 18% (26 mg). The obtained product was, however, not stable. Therefore, column chromatography was not performed in the second run and the resulting product was used as such for the next step. ¹H-NMR (400 MHz, CDCl₃), δ(ppm): 7.55 (d, *J* = 5.2 Hz, 1H), 6.89 (s, 1H), 6.76 (d, *J* = 5.2 Hz, 1H), 3.67–3.66 (m, 4H), 3.60 (s, 1H), 1.90–1.80 (br, 2H) 1.40–1.18 (br, 64H), 0.89–0.82 (m, 12H).

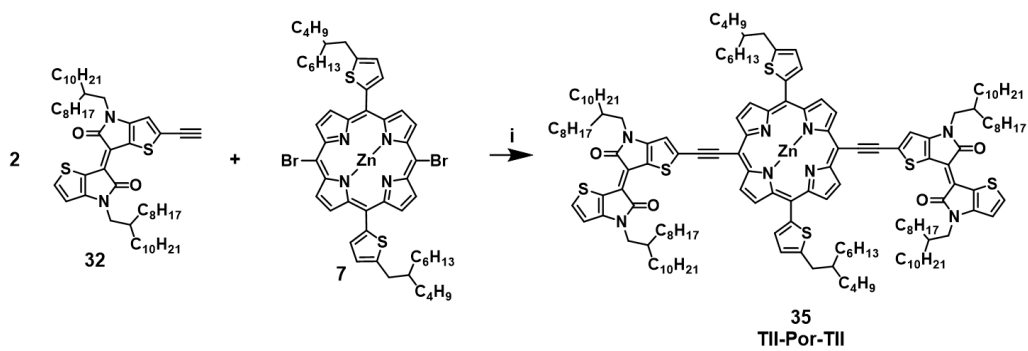
4-(5-ethynyl-4-hexylthiophen-2-yl)-9-(4-hexylthiophen-2-yl)-6,7-di(thiophen-2-yl)-

[1,2,5]thiadiazolo[3,4-*g*]quinoxaline (33). Due to degradation occurring during the reaction and/or purification, the target molecule could not be obtained.

4-(5-ethynyl-4-(2-octyldodecyl)thiophen-2-yl)-8-(4-(2-octyldodecyl)thiophen-2-yl)-1H,5H-benzo-

[1,2-*c*:4,5-*c'*]bis([1,2,5]thiadiazole) (34). Due to degradation occurring during the reaction and/or purification, the target molecule could not be obtained.

Sonogashira cross-coupling procedure toward TII-Por-TII (35). A₂B₂-porphyrin precursor **7** (1 equiv.) and the mono-alkynated acceptor molecule **32** (2.2 equiv.) were placed in a Schlenk flask and the flask was flushed three times with N₂, after which dry toluene (7.3 mM) and dry Et₃N (3.7 mM) were added. Then, the mixture was purged with N₂ for 30 min. Afterwards, Pd(PPh₃)₂Cl₂ (0.05 equiv.) and CuI (0.05 equiv.) were added and the reaction was stirred overnight at 85 °C. Next morning, the reaction mixture was cooled down, water was added and extraction was done with CHCl₃. The organic solution was dried over MgSO₄, filtered and evaporated to dryness. Flash column chromatography (silica) was performed with CHCl₃:petroleum ether (3:1). Further purification was not performed due to the multitude of reaction products obtained, as evidenced by MALDI-ToF mass spectrometry (Figure S26).



Scheme S10: Final Sonogashira cross-coupling yielding **TII-Por-TII (35)**: i) $\text{PdCl}_2(\text{PPh}_3)_2$, CuI , Et_3N , toluene, 85°C .

3.3. $^1\text{H-NMR}$, $^{13}\text{C-NMR}$, and MALDI-ToF mass spectra

(*E*)-2-bromo-4,4'-bis(2-octyldodecyl)-[6,6'-bithieno[3,2-*b*]pyrrolylidene]-5,5'(4*H*,4'*H*)-dione (25)

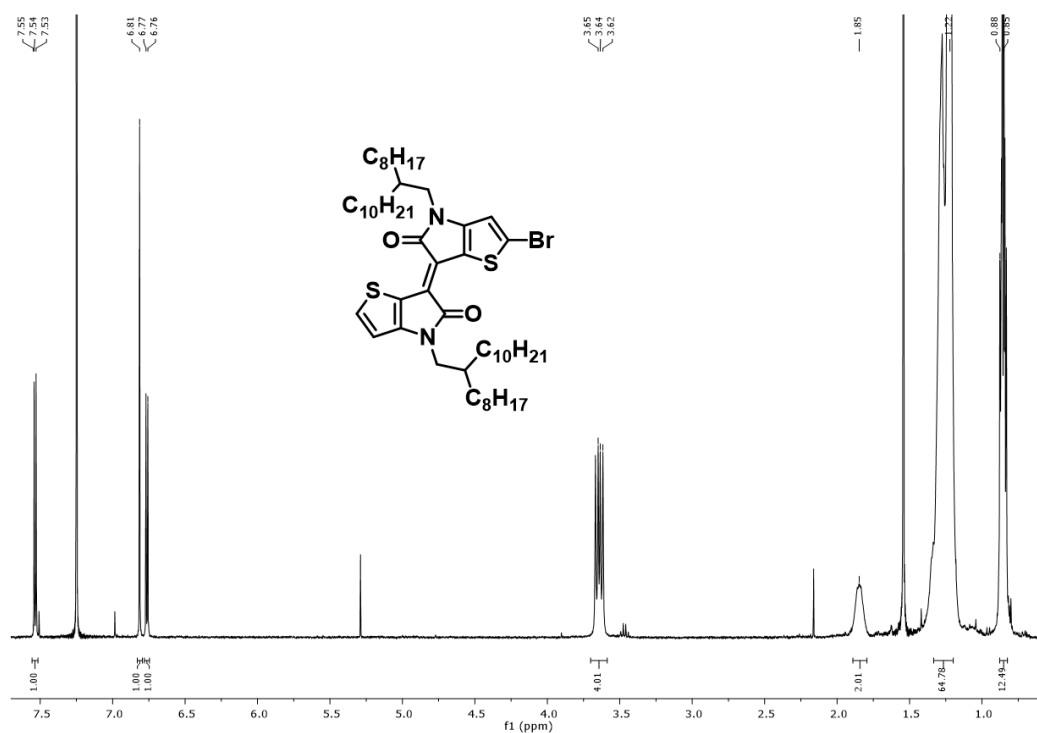


Figure S26: $^1\text{H-NMR}$ spectrum of compound 25.

4-(5-bromo-4-hexylthiophen-2-yl)-9-(4-hexylthiophen-2-yl)-6,7-di(thiophen-2-yl)-[1,2,5]thiadiazolo[3,4-*g*]quinoxaline (26)

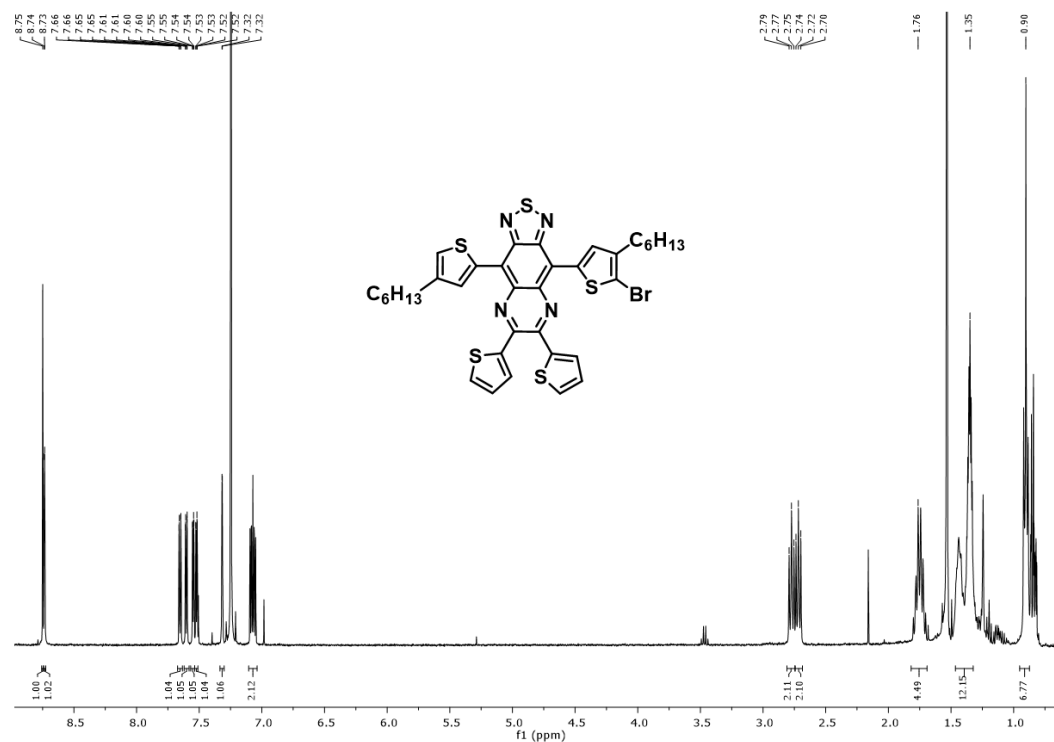


Figure S27: $^1\text{H-NMR}$ spectrum of compound 26.

(E)-4,4'-bis(2-octyldodecyl)-2-((trimethylsilyl)ethynyl)-[6,6'-bithieno[3,2-*b*]pyrrolylidene]-5,5'(4*H*,4'*H*)-dione (29)

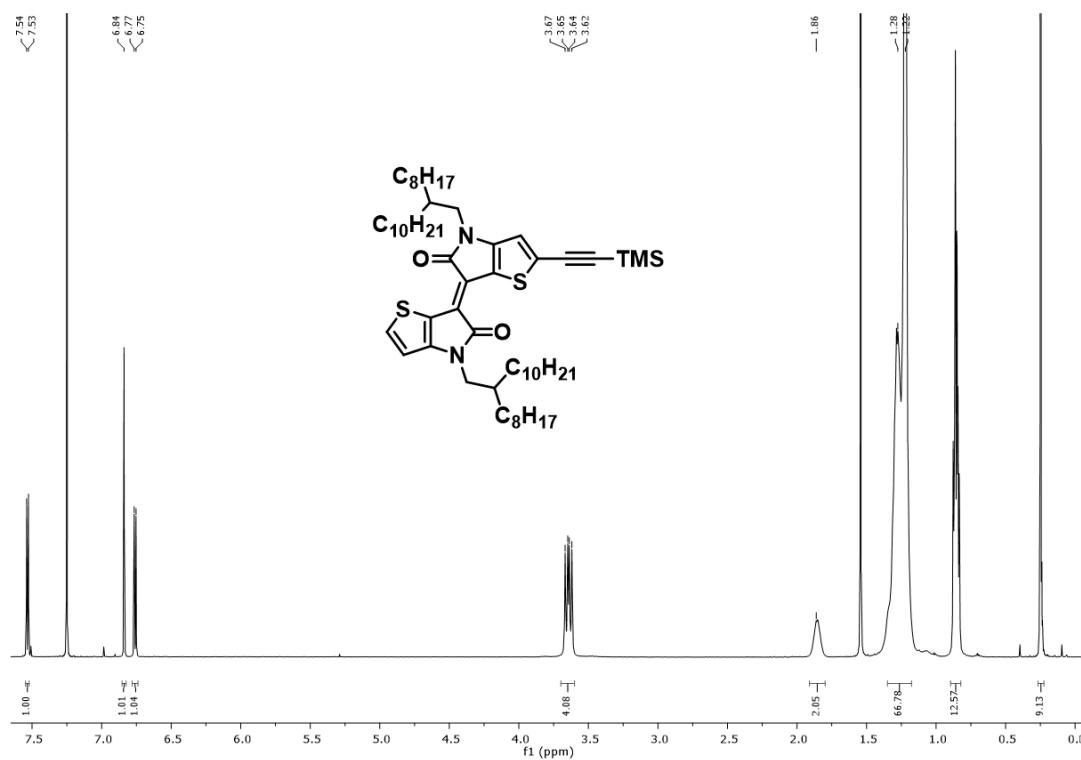


Figure S28: ¹H-NMR spectrum of compound 29.

4-(4-hexyl-5-((trimethylsilyl)ethynyl)thiophen-2-yl)-9-(4-hexylthiophen-2-yl)-6,7-di(thiophen-2-yl)-[1,2,5]thiadiazolo[3,4-*g*]quinoxaline (30)

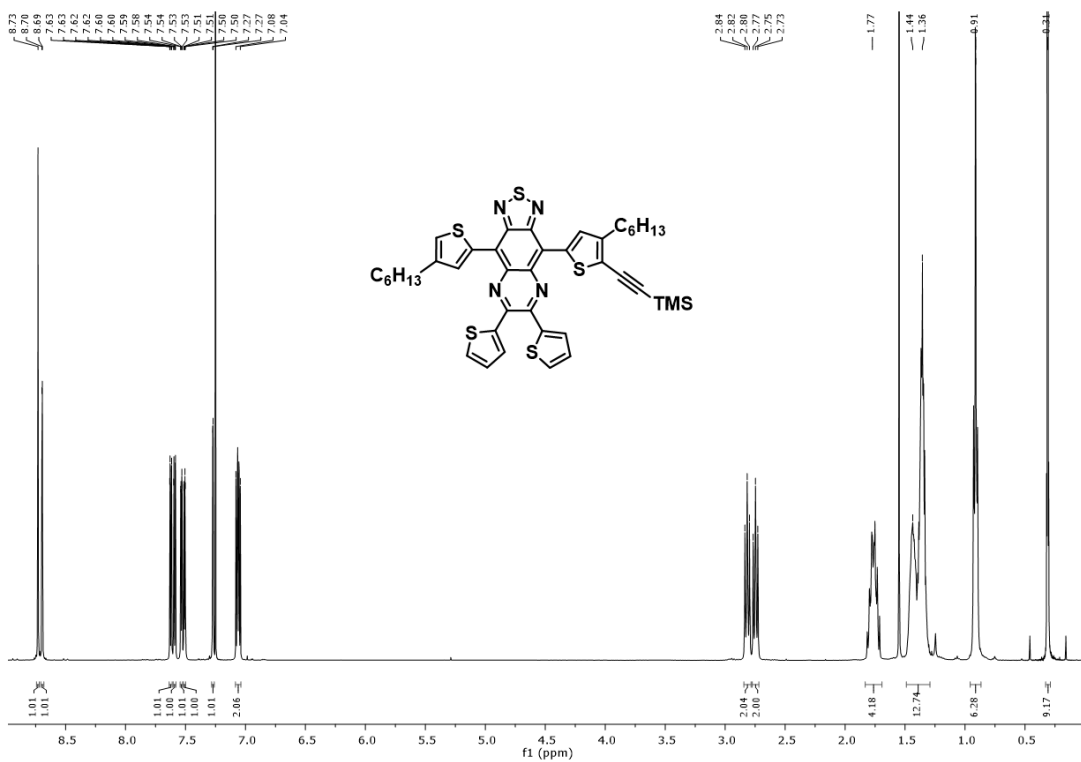


Figure S29: ¹H-NMR spectrum of compound 30.

4-(4-(2-octyldodecyl)-5-((trimethylsilyl)ethynyl)thiophen-2-yl)-8-(4-(2-octyldodecyl)thiophen-2-yl)-1*H*,5*H*-benzo[1,2-*c*:4,5-*c'*]bis[[1,2,5]thiadiazole) (31)

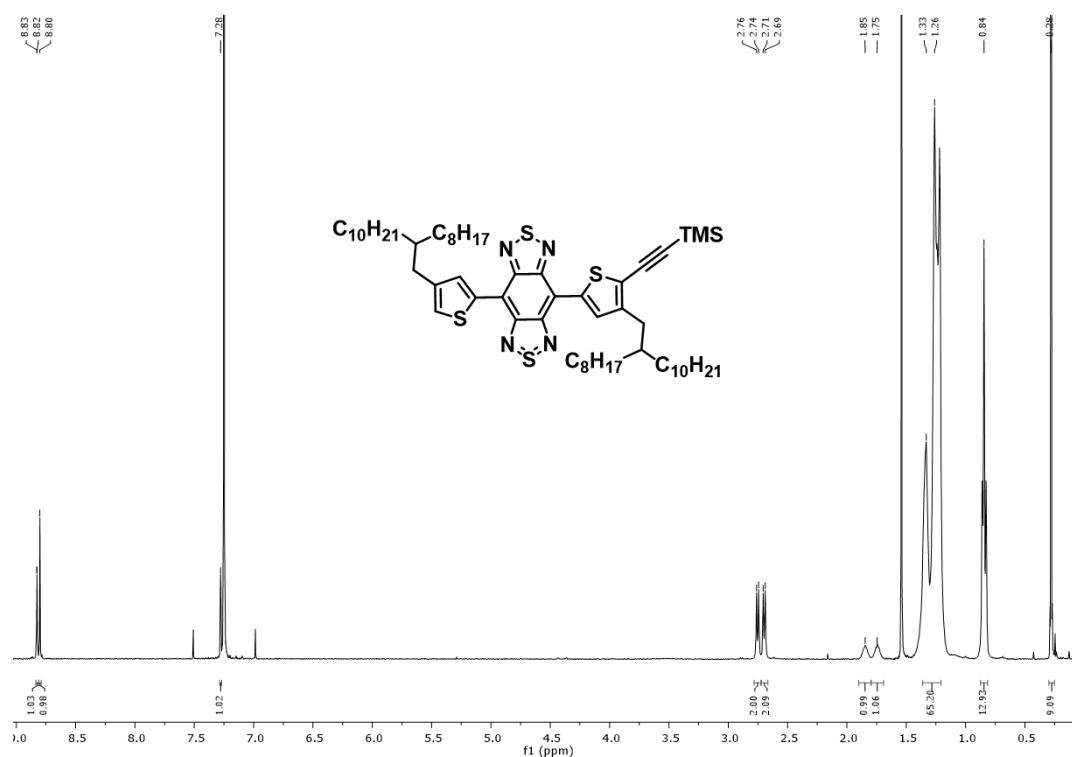


Figure S30: ¹H-NMR spectrum of compound **31**.

(*E*)-2-ethynyl-4,4'-bis(2-octyldodecyl)-[6,6'-bithieno[3,2-*b*]pyrrolylidene]-5,5'-(4*H*,4'*H*)-dione (32)

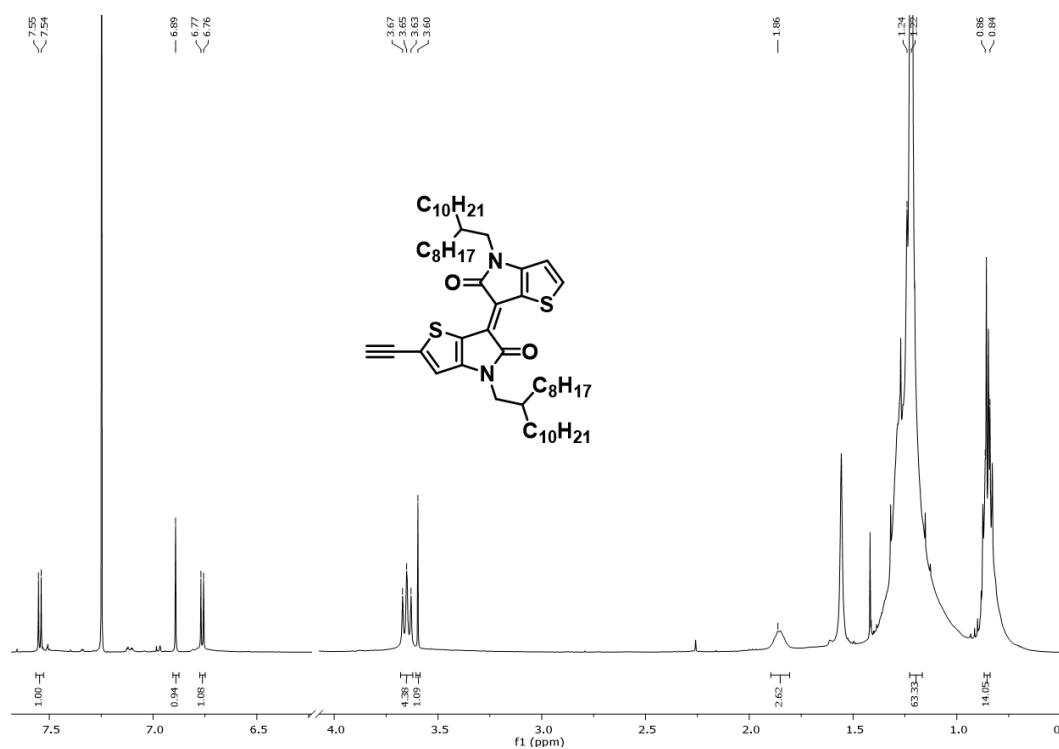


Figure S31: ¹H-NMR spectrum of the alkynated thienoisindigo **32** after deprotection (without purification).

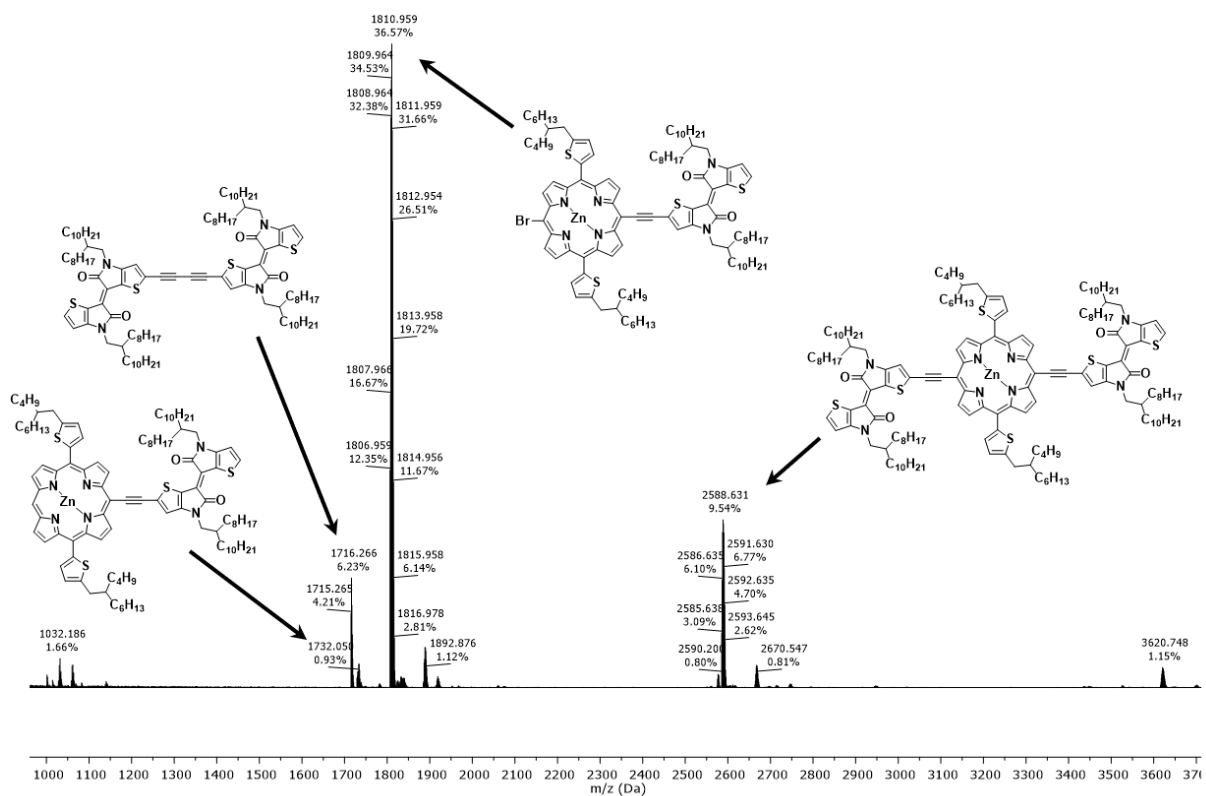


Figure S32: MALDI-ToF mass spectrum of the crude product resulting from the Sonogashira cross-coupling reaction of porphyrin **7** and alkynated TII **32**. Plausible molecular structures are shown for the different masses observed.

References

- 1 S. Trasatti, *Journal of Electroanalytical Chemistry and Interfacial Electrochemistry*, 1986, **209**, 417.
- 2 A. J. Bard, L. R. Faulkner, *Electrochemical Methods: Fundamentals and Applications*, 2nd edition, Wiley, 2000.
- 3 K. Gao, J. Miao, L. Xiao, W. Deng, Y. Kan, T. Liang, C. Wang, F. Huang, J. Peng, Y. Cao, F. Liu, T. P. Russell, H. Wu, X. Peng, *Advanced Materials*, 2016, **28**, 4727.
- 4 V. Cuesta, R. Singhal, P. de la Cruz, G. D. Sharma, F. Langa, *ACS Applied Materials & Interfaces*, 2019, **11**, 7216.
- 5 J. Fan, J. D. Yuen, M. Wang, J. Seifert, J.-H. Seo, A. R. Mohebbi, D. Zakhidov, A. Heeger, F. Wudl, *Advanced Materials*, 2012, **24**, 2186.
- 6 M. Karikomi, C. Kitamura, S. Tanaka, Y. Yamashita, *Journal of the American Chemical Society*, 1995, **117**, 6791.
- 7 F. Verstraeten, S. Gielen, P. Verstappen, J. Raymakers, H. Penxten, L. Lutsen, K. Vandewal, W. Maes, *Journal of Materials Chemistry C*, 2020, **8**, 10098.
- 8 S. Gielen, C. Kaiser, F. Verstraeten, J. Kublitski, J. Benduhn, D. Spoltore, P. Verstappen, W. Maes, P. Meredith, A. Armin, K. Vandewal, *Advanced Materials*, 2020, **32**, 2003818.
- 9 J. Ilavsky, *J. Appl. Cryst.*, 2012, **45**, 324.
- 10 S. Oosterhout, V. Savikhin, J. Zhang, Y. Zhang, M. Burgers, S. Marder, G. Bazan, M. Toney, *Chem. Mater.*, 2017, **29**, 3062.
- 11 J. Kesters, P. Verstappen, M. Kelchtermans, L. Lutsen, D. Vanderzande, W. Maes, *Advanced Energy Materials*, 2015, **5**, 1500218.
- 12 A. K. K. Kyaw, D. H. Wang, C. Luo, Y. Cao, T.-Q. Nguyen, G. C. Bazan, A. J. Heeger, *Advanced Energy Materials*, 2014, **4**, 1301469.
- 13 G. W. P. Van Pruissen, F. Gholamrezaie, M. M. Wienk, R. A. J. Janssen, *Journal of Materials Chemistry*, 2012, **22**, 20387.
- 14 M. C. Ruiz Delgado, V. Hernández, J. T. López Navarrete, S. Tanaka, Y. Yamashita, *The Journal of Physical Chemistry B*, 2004, **108**, 2516.
- 15 M. L. Keshtov, L. Toppare, D. V. Marochkin, V. S. Kochurov, D. Y. Parashchuk, V. A. Trukhanov, A. R. Khokhlov, *Polymer Science Series B*, 2013, **55**, 360.